Size characterization of airborne SiO$_2$ nanoparticles with on-line and off-line measurement techniques: an interlaboratory comparison study

C. Motzkus · T. Macé · F. Gaie-Levrel · S. Ducourtieux · A. Delvallee ·
K. Dirscherl · V.-D. Hodoroaba · I. Popov · O. Popov · I. Kuselman ·
K. Takahata · K. Ehara · P. Ausset · M. Maillé · N. Michielsen · S. Bondiguel ·
F. Gensdarmes · L. Morawska · G. R. Johnson · E. M. Faghihi · C. S. Kim ·
Y. H. Kim · M. C. Chu · J. A. Guardado · A. Salas · G. Capannelli ·
C. Costa · T. Bostrom · Å. K. Jämting · M. A. Lawn · L. Adlem · S. Vaslin-Reimann

Abstract Results of an interlaboratory comparison on size characterization of SiO$_2$ airborne nanoparticles using on-line and off-line measurement techniques are discussed. This study was performed in the framework of Technical Working Area (TWA) 34—"Properties of Nanoparticle Populations" of the Versailles Project on Advanced Materials and Standards (VAMAS) in the project no. 3 "Techniques for characterizing size distribution of airborne nanoparticles". Two types of nano-aerosols, consisting of (1) one population of nanoparticles with a mean diameter between 30.3 and 39.0 nm and (2) two populations of non-agglomerated nanoparticles with mean diameters between, respectively, 36.2–46.6 nm and 80.2–89.8 nm, were generated for characterization measurements. Scanning mobility particle size spectrometers (SMPS) were used for on-line measurements of size distributions of the produced nano-aerosols. Transmission electron microscopy, scanning electron microscopy, and atomic force microscopy were used as off-line measurement

C. Motzkus (✉) · T. Macé · F. Gaie-Levrel ·
S. Ducourtieux · A. Delvallee · S. Vaslin-Reimann
Laboratoire National de Métrologie et d'Essais (LNE), 1
rue Gaston Boissier, 75724 Paris Cedex 15, France
e-mail: charles.motzkus@lne.fr

K. Dirscherl
Danish Fundamental Metrology (DFM), Matematiktorvet
307, 2800 Kgs. Lyngby, Denmark

V.-D. Hodoroaba
BAM Federal Institute for Materials Research and
Testing, 12200 Berlin, Germany

I. Popov
Unit for Nanocharacterization, The Hebrew University of
Jerusalem, Supply Dept Building Ground Floor, Givat
Ram, 91904 Jerusalem, Israel

O. Popov · I. Kuselman
National Physical Laboratory of Israel (INPL), Danciger
"A" Bldg, Givat Ram, 91904 Jerusalem, Israel

K. Takahata · K. Ehara
National Metrology Institute of Japan (NMIJ), National
Institute of Advanced Industrial Science and Technology
(AIST), 1-1-1 Umezono, Tsukuba, Ibaraki 305-8563,
Japan

P. Ausset · M. Maillé
Laboratoire Interuniversitaire des Systèmes
Atmosphériques (LISA), UMR CNRS 7583, Université
Paris-Est Créteil et Université Paris-Diderot, 61 Avenue
du Général de Gaulle, 94010 Créteil, France

N. Michielsen · S. Bondiguel · F. Gensdarmes
PSN-RES, SCA, LPMA, Institut de Radioprotection et de
Sûreté Nucléaire (IRSN), Saclay, 91192 Gif-sur-Yvette,
France

L. Morawska · G. R. Johnson · E. M. Faghihi
International Laboratory for Air Quality and Health
(ILAQH), Queensland University of Technology (QUT),
2 George Street, Brisbane, QLD 4001, Australia

techniques for nanoparticles characterization. Samples were deposited on appropriate supports such as grids, filters, and mica plates by electrostatic precipitation and a filtration technique using SMPS controlled generation upstream. The results of the main size distribution parameters (mean and mode diameters), obtained from several laboratories, were compared based on metrological approaches including metrological traceability, calibration, and evaluation of the measurement uncertainty. Internationally harmonized measurement procedures for airborne SiO_2 nanoparticles characterization are proposed.

Introduction

Nanotechnology is one of the six Key Enabling Technologies (KETs) selected by the European Commission as producing a major economic impact and societal challenges (EC 2009, 2011a, b). Indeed, the probability of finding nano-objects in the workplace, as well as in ambient air, increases with the development of new industrial applications of nanotechnology employing nanomaterials in the car industry, electronics, communications, cosmetics, energy, environment, pharmaceutical biomedicine, and bio-technology. Scientific studies of health and environmental risks indicated that nano-objects, in particular in aerosol form, have potentially adverse health effects on exposed workers and the general population (Oberdörster 2001; Maynard and Kuempel 2005; Oberdörster et al. 2005; Witschger and Fabriès 2005; Nel et al. 2006; Tsuji et al. 2006; AFFSET 2006, Lahmani et al. 2010). With regard to these risks, three potential routes of exposure were identified: ingestion, epidermal absorption, and inhalation. The last one is considered as predominant, especially in the workplace (Witschger et al. 2012).

Relevant characteristics of airborne nanoparticles, such as the particle size (ISO 2011), strongly influence the particle deposition in the respiratory tract (ISO 2007, 2012). Up to now, the knowledge of the impact on people's health, following exposure to nanomaterials inhalation, is incomplete. In order to address societal issues around nano-objects, standardized characterization protocols for traceable and reliable measurements are necessary (Maynard et al. 2006; Maynard and Pui 2007). Therefore, a number of interlaboratory comparisons have been performed over the last 20 years with on-line and off-line techniques in order to measure particle parameters (Cadle and Mulawa 1990; Countess 1990; Schmid et al. 2011; Zervas et al. 2005; Hering et al. 1990; Slowik et al. 2007). In such studies, sampling for off-line particle measurements is a crucial step to obtain representative, reliable analysis results. A recent study of Cyrs et al. (2010) focused on the nanoparticle collection efficiency of capillary pore membrane filters (PMFs). The authors pointed out that size-specific correction factors could be used for characterization of the particle size distribution (PSD) of airborne particles measured by microscopy techniques.

The major conclusion of these inter-laboratory comparison studies was on the lack of measurement standards and of harmonized and standardized measurement procedures. As an example, Cadle and Mulawa

C. S. Kim · Y. H. Kim · M. C. Chu
Division of Industrial Metrology, Korea Research Institute of Standards and Science (KRISS), 1 Doryong-Dong, Yuseong-Gu, Taejon 305-340, Korea

J. A. Guardado · A. Salas
Area de Metrología de Materiales, Centro Nacional de Metrología (CENAM), Carretera a los Cués km 4,5, 76246 El Marqués, QRO, Mexico

G. Capannelli · C. Costa
Department of Chemistry and Industrial Chemistry, University of Genoa (UNIGE), via Dodecaneso 31, 16146 Genoa, Italy

T. Bostrom
Science and Engineering Faculty, Queensland University of Technology (QUT), GPO Box 2434, Brisbane, QLD 4001, Australia

Å. K. Jämting · M. A. Lawn
National Measurement Institute Australia (NMIA), PO Box 264, Lindfield, NSW 2070, Australia

L. Adlem
National Metrology Institute of South Africa (NMISA), Private Bag X34, Lynnwood Ridge 0040, South Africa

(1990) concluded that their measurement accuracy is unknown, since measurement standards of elementary carbon in atmospheric particles do not exist. Zervas et al. (2005) pointed out that only metrological aspects such as measurement repeatability and detection limits were studied in their work, without considering calibration of the measuring instruments. During their interlaboratory study performed in a vehicle and involving a reference particle measurement system, Giechaskiel et al. (2008) pointed out that calibration procedures for such an instrument should be better defined.

Other interlaboratory comparisons have been performed in order to compare off-line measurement techniques, such as proton-induced X-ray emission, X-ray fluorescence (Calzolai et al. 2008), and on-line techniques, such as mobility particle size spectrometers (MPS) (Wiedensohler et al. 1993; Rodrigue et al. 2007). The performances of four scanning mobility particle size spectrometers (SMPS) were evaluated by Fissan et al. (1996) under the same conditions for flow rates, flow ratio, input monodisperse aerosols, and transport-line lengths in the 6–50 nm size range. Their results provide a quantitative comparison of the mobility resolution and diffusion loss of the nanometer aerosols in such systems. Moreover, the performance assessment of Fast MPS (FMPS) and Ultrafine Water-based Condensation Particle Counter (UWCPC) equipped SMPS was performed by Jeong and Evans (2009) under various conditions on urban ambient particles, urban indoor particles, rural ambient particles, and laboratory-generated particles. Asbach et al. (2009) tested four different mobility particle sizers on NaCl and diesel soot particles measurements.

A lack of metrological traceability can therefore be identified in these studies, so the need of traceable measurement results becomes of crucial importance. Only the paper of Wiedensohler et al. (2012) talks about harmonization of measurement procedures to facilitate high quality long-term observations of atmospheric particle size number distributions obtained by SMPS.

In this paper, we present results of a study performed within the framework of Technical Working Area (TWA) no. 34—"Properties of Nanoparticle Populations" of the Versailles Project on Advanced Materials and Standards (VAMAS) in project no. 3 "Techniques for characterizing size distribution of airborne nanoparticles". The working group of this project is composed of 11 National Metrology Institutes (BAM, CENAM, DFM, NMIA, NMISA, INPL, KRISS, LNE, NIST,

NMIJ-AIST, NPLI) and four laboratories involved in nanoparticle metrology (LPMA, LISA, [ILAQH-QUT], UNIGE). This work was focused on manufactured SiO_2 nanoparticles because of their widespread use in industry. Two types of non-agglomerated nano-aerosols (Motzkus et al. 2010, 2011, 2012) were generated. One contained a single population of nanoparticles, and the second one was composed of two populations of non-agglomerated nanoparticles. The results, presented in this paper, were obtained during an interlaboratory comparison for SiO_2 airborne nanoparticles characterization using (1) an on-line measurement technique, called SMPS (described as a Differential Mobility Analysing System by ISO 2009), and (2) off-line measurement techniques, namely transmission electron microscopy (TEM), scanning electron microscopy (SEM), and atomic force microscopy (AFM), all of which needed the particles collection on appropriate supports (grids, filters and mica plates). Based on these results, international harmonized measurement procedures for size characterization of airborne SiO_2 nanoparticles are proposed.

Measurement methods

Five SMPS laboratories were involved in this study in order to compare different aerosol generation methods and to evaluate interlaboratory variation of the SMPS PSD measurements (coded SMPS1-5). Seven other laboratories participated in TEM analysis, seven in SEM, and four in AFM measurements, in order to compare parameters of the size distributions obtained by these techniques for aerosol particles deposited on grids, filters, and mica plates by electrostatic precipitation and filtration techniques used during the SMPS controlled generation upstream.

Nano-aerosol generation and on-line measurement

The objectives were to generate airborne SiO_2 nanoparticles and to characterize the PSD of the generated aerosols with different on-line measurement techniques, and to validate them by an interlaboratory comparison.

Aerosol generation set-up and on-line measurement systems

The instruments used for the interlaboratory comparison were an aerosol generator, a differential mobility

analyser (DMA), and a condensation particle counter (CPC). An atomizer, available to the greatest number of participants, was used to generate high concentration aerosols. Electrospray was also used by the fifth SMPS laboratory as a generation system to produce nano-aerosols with fewer impurities (parasitic particles), compared to the atomizer. The same DMA commercial type (model 3080, TSI) was used by all participants. DMA was operated in (1) scanning mode, and (2) stepping mode. In the scanning mode, the commercial software, Aerosol Instrument Manager (AIM), was used for DMA control and data analysis. DMA flows were selected for a wide particle size range in order to monitor and assess trends in particle generation. For the stepping mode, custom-made software was used for DMA control and data analysis based on the DMA moment method (Ehara et al. 2000). DMA flows were selected to obtain the best resolution to determine the PSD parameters. Different types of CPC, used in this study, were also commercial devices from the TSI company. Each CPC was connected to a DMA using tubes with a length of 25 cm and a diameter of 6 mm. Figure 1 shows the most common set-up and specific details of the different systems used by the SMPS laboratories. Table 3 in Appendix lists associated operating parameters.

The analysis steps described in "Determination of particle size distribution—Differential electrical mobility analysis for aerosol particles" (ISO 15900 2009) for DMA were taken into account. Calibrations for size measurements were performed using Certified Reference Materials (CRMs) of *Polystyrene Latex* particles (PSL CRMs) certified by TEM [46 ± 2 nm (3050A, Thermo Fisher Scientific), 81 ± 3 nm (3080A, Thermo Fisher Scientific) and 100.82 ± 0.66 nm (STADEX SC-010-S, JSR)]. The calibration results are listed in Table 3.

Airborne SiO$_2$ nanoparticles generation protocol

Sample preparation with colloidal suspensions   The best available purified and deionized water was used to prepare diluted suspensions. In order to obtain an aerosol with one nanoparticle population (a monomodal PSD), an amount of a manufactured colloidal suspension was diluted in 1 l of Milli-Q water. This prepared solution was then introduced into the bottle of an atomizer system (model 3076, TSI) in order to obtain a monodisperse population called "Aerosol One Population" (aerosol OP). To produce an aerosol with two nanoparticle populations (a bimodal PSD), 50 µL of a second manufactured colloidal suspension was
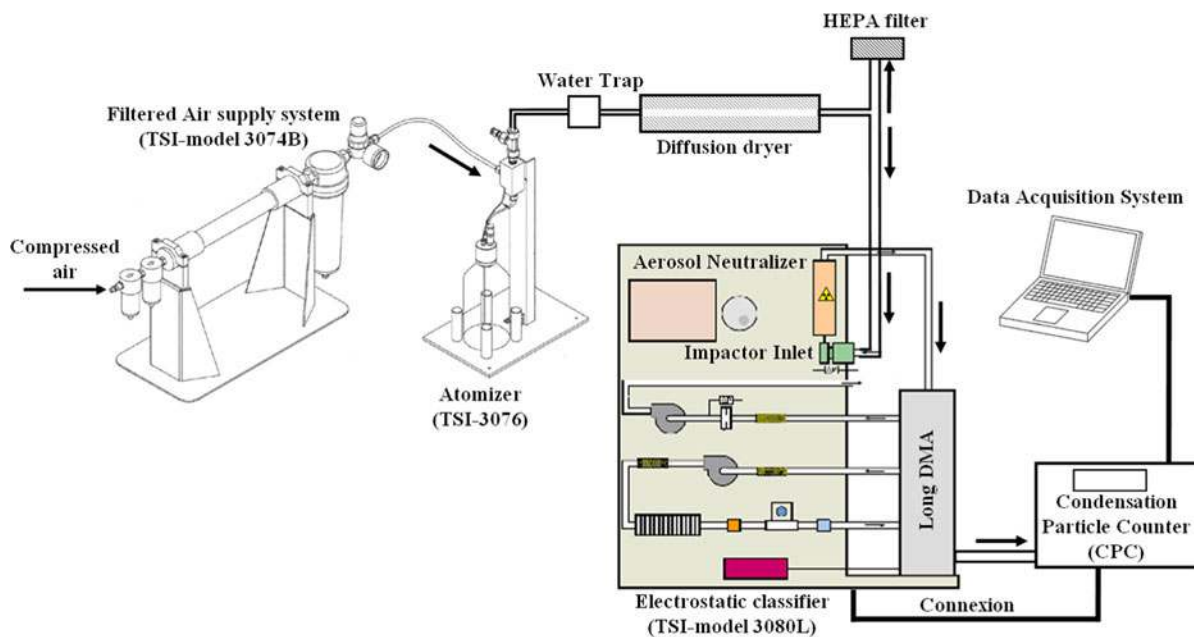

Fig. 1 Setup of generation and size characterization of SiO$_2$ airborne nanoparticles available to the greatest number of laboratories

diluted in 1 l of Milli-Q water. This prepared solution was then introduced into the bottle of an identical atomizer system (model 3076, TSI) in order to obtain a double-population aerosol called "Aerosol Double Population" (aerosol DP) characterized by two populations of isolated (non-agglomerated) airborne particles.

The SiO_2 manufactured colloidal suspensions were chosen according to their properties (particle size, morphology, and agglomeration state) and their availability. The first suspension contained a single population of nanoparticles, and the second one was composed of two populations with particle size below 100 nm of non-agglomerated nanoparticles with spherical shape. The values of the aspect ratio (minimum feret diameter divided by maximum feret diameter) of the particles as measured by TEM are in the range between 0.92 and 0.96 indicating a relatively high sphericity of the nanoparticles.

The samples were distributed to the participants knowing that all the samples were coming from the same batch. Special attention was taken during transportation by using tightly sealed containers to prevent evaporation and to ensure the sample integrity.

Aerosol generation Before each generation of SiO_2 nanoparticles, the aerosol background was checked by nebulising the solvent alone (water) after by cleaning the bottle and the atomizer three times with Milli-Q water. This was performed until the background resulting from remaining SiO_2 particles was negligible. Each aerosol generator was used under optimum conditions. For example, a TSI atomizer 3076 was operated at a pressure of 2.4 bars of clean-dry air delivered from a commercial device (model 3074B, TSI). Generated particles are then introduced through a homogenization chamber and a solvent collection tank before passing through diffusion driers and analysis by on-line SMPS device.

SMPS measurement methods

Scanning mode: operating parameters and software Aerosol Instrument Manager (AIM) software (Release Version 8.1.0.0, TSI) was used with or without diffusion and charge corrections. A density of 2.2 and 1.2×10^{-3} g/cm^3 for particles and gas, respectively, was taken into account. Different sheath (q_c) and aerosol (q_a) flows were used. These flow conditions corresponded to a 14–673 nm size range. The

scanning steps were identical, 180 s for voltage increasing, 30 s for voltage decreasing and the remaining 30 s for idling, with a total recording time of 4 min. The measurements were started only when the generation system was stable for longer than 10 min, and at least 10 scans were recorded on three different days.

Stepping mode: operating parameters and DMA moment method For the stepping mode, DMA flows were set at $q_c = 19.5$ L/min and $q_a = 1.0$ L/min. The CPC (model 3022A, TSI), which is used to count particles at the DMA exit, was operated in the low flow mode (0.3 L/min). At least eleven values for DMA voltages were selected to cover the whole particle peak. Each voltage was applied for 30 s with the first 20 s for idling and the remaining 10 s for particle counting. The measurement was started from the voltage which was expected to be close to the middle of the peak. The voltage was then changed alternately to the left and to the right of this first voltage, knowing that the first and last voltages should match in order to check the stability of aerosol generation. It was considered that the DMA spectrum had to be done again when the difference between first and last particles counts was larger than 10 %.

Curve fitting was employed to obtain the size distribution. In these conditions, the peak was clearly isolated from background particles and the average diameter could be determined. The peak voltage diameter was also determined in order to compare the obtained mode diameter with the one obtained by scanning mode operation. Furthermore, the certified diameter of the reference particles was used to correct possible errors in DMA electrode dimensions. For each sample, the measurements were repeated three times on three different days. The equations given by Allen and Raabe (1985) and established by Wiedensohler (1988) were used, respectively, for the slip correction and equilibrium charge distribution.

Results treatment and uncertainty measurement

The measurement results were treated according to the ISO 5725-2 (ISO 1994) procedure in order to determine repeatability and reproducibility of mean and mode diameters for each particle population. Gaussian (normal), asymmetric Gaussian, and log-normal distribution models were used. The influence of different aerosol generators, DMA flow conditions, and the

presence or absence of diffusion and charge corrections were investigated to evaluate measurement uncertainty components and to calculate the expanded uncertainty. In order to better describe aerosol DP, two ratios in number concentration were calculated. The peak and area ratios correspond, respectively, to the ratio of the maximum intensities (mode, in number concentration) and to the ratio of the two populations areas, either in integrality (Gaussian law) or integrated on determined size ranges.

Sampling for off-line measurements

As mentioned above, TEM, SEM, and AFM were used as off-line techniques to measure the number-based PSD of SiO_2 airborne nanoparticles collected on appropriate supports after their generation. Concerning the SMPS-controlled nanoparticles generation, identical protocols as described in "Nano-aerosol generation and on-line measurement" were used, and either a flow splitter connection (model 3708, TSI) or a T-junction were used, depending on the laboratories for SMPS and off-line sampling systems connections. In this study, two main sampling techniques were used: electrostatic precipitation and filtration.

Sampling methods

Electrostatic precipitation Electrostatic precipitation (Bau et al. 2010; Li et al. 2010; Dixkens and Fissan 1999) can also be performed to sample airborne nanoparticles. In this study, a Nanometer Aerosol Sampler (NAS, Model 3089, TSI) was used to collect SiO_2 nanoparticles. For the off-line analysis study, mica substrates (AGAR Scientific, G250-3, 11×11 mm, roughness ~ 50 pm, root mean square roughness 0.08 nm) and TEM grids (Formvar carbon on 200 mesh Cu grid and pure carbon on 200 mesh Cu grid), fixed with liquid silver glue on a 9.5-mm NAS electrode, were used. Before each sampling, the NAS chamber and its electrode were cleaned with ethanol and dried with filtered compressed air. A flow rate of 2 L/min and a voltage of 10 kV were used for the sampling in order to obtain a high collection efficiency and the greatest amount of collected nanoparticles. It was recommended to deposit SiO_2 nanoparticles onto the shiny side of the TEM grids (Formvar/Carbon film). Just before deposition, the mica must be cleaved

using the adhesive tape method until the surface appears visually featureless. Two TEM grids of different types were used in this study and were labeled N1, N2 for carbon-coated Formvar films and N3, N4 for pure carbon film. The TEM grids with pure carbon were required for AFM measurements due to the fragility of Formvar-carbon films rendering them unsuitable for AFM scanning. Each sampling laboratory took at least two TEM grids of each type in order to study the repeatability of their sampling process.

Two configurations of the NAS system connection were used in this study, i.e. before (configuration 1) and after (configuration 2) the Kr85 SMPS neutralizer. A preliminary study shows that configuration 1 was better suited to collect generated SiO_2 airborne nanoparticles on TEM grids than configuration 2, due to the higher particle concentration and the associated reduction of sampling time. The other advantage of this configuration was the possibility to easily connect the SMPS in parallel in order to control the size distribution of the produced aerosol. For configuration 1, sampling times of 5 min and 2 min 30 s on TEM grids were used for both SiO_2 nano-aerosols (OP and DP) and a sampling time of 30 min for mica substrates in order to obtain a suitable nanoparticle surface density (~ 20 particles/μm^2). This allowed maximizing the number of collected particles without particle overlaps. For configuration 2, sampling time was 2 h. The mica and TEM grids samples obtained using the NAS system are, respectively, called samples D and B. Each sampling laboratory produced three mica samples for each AFM laboratory (called M1, M2 and M3) in order to study the repeatability of their sampling process.

Filtration technique Filtration is a technique which uses diffusion, interception, and impaction processes to collect particles on a substrate. Diffusion is the major phenomenon involved in deposition of airborne nanoparticles.

Airborne SiO_2 nanoparticles were sampled using a 25-mm filter holder equipped with a pump and a regulator in order to control the flow rate at 2 L/min. Before each sampling, the filter holder was cleaned with ethanol and dried with filtered compressed air. Sampling was performed simultaneously on 25 mm polycarbonate membrane filters (PMF, Nuclepore®) with pore size of 0.2 μm and on 3 mm TEM grids placed directly on the PMF. Two TEM grids (G1 and

G2, carbon-coated Formvar film and pure carbon film on 200 mesh Cu grids), placed at a radial distance of 6.5 mm from the PMF centre, were used and called "sample A" (Fig. 2) for TEM and AFM measurements. After sampling, PMFs were cut for TEM (piece P1, Fig. 2) and SEM (Piece P2, Fig. 2) analysis.

Preliminary tests showed that particle density on the filter is higher than for TEM grids. Therefore, other PMFs without TEM grids and with lower particle density were used to avoid particle overlaps (sample C, Fig. 2). Each sampling laboratory produced three A and C samples (F1, F2, and F3) for SEM and TEM measurements in order to study the repeatability of their sampling process. Moreover, several laboratories had the opportunity to transfer nanoparticles first deposited on A and C PMF samples to TEM grids (g1 and g2, respectively, on carbon-coated Formvar films and pure carbon film on 200 mesh Cu grids) via its dissolution (Fig. 2) in order to estimate the impact of this method on the measurement.

For samples A, sampling times of 10 and 5 h were used, respectively, for aerosols OP and DP, in order to obtain good nanoparticle density ($\sim$20–50 particles/μm^2) on the TEM grids and no particle overlaps. For samples C, sampling times of 12 and 15 min were used, respectively, for aerosols OP and DP, in order to obtain particle densities of 15–30 particles/μm^2 on the PMF.

Storage conditions and sample transport

After sampling, each filter was placed in a numbered polypropylene petri dish (Petrislides type) for storage and transport. TEM grids were placed in numbered holes of a grid box. The shiny side was turned towards the left side of the holes wall. Mica substrates were prepared for transport and AFM measurements by sticking them to steel discs (20 mm metal specimen discs, Ted Pella). The samples were transported in an atmosphere with a relative humidity below 30 % in vacuum plastic boxes in order to prevent pollution from ambient air. The boxes were equipped with a magnetic tape at the bottom to attach the steel discs and to facilitate easy removal. The sample batches were stored under dark conditions in vacuum boxes with bubble packs to reduce shocks and vibrations during transport.

Off-line technique interlaboratory comparison organization

Each sampling laboratory collected three samples (M, G, F, see "Sampling methods" section) of A, B, C, and D sample types, for at least two different AFM, TEM, and SEM microscopy laboratories, in order to study homogeneity, repeatability of the sampling, and interlaboratory variability of the measurement methods

Fig. 2 Description of the sampling methods used for TEM and SEM analysis. The associated nomenclatures are indicated for sample A (*left*) and sample C (*right*)
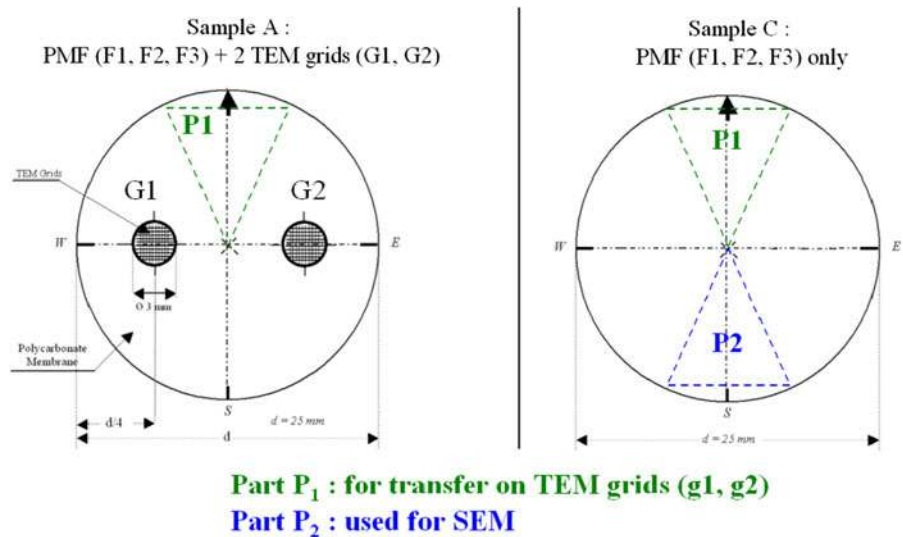
applied in each microscopy laboratory (ISO 17043 2010). AFM laboratories analyzed some TEM grids (from TEM laboratories) only for A and B samples.

Off-line microscopy analysis

Atomic force microscopy

After their generation and sampling on either mica or grids, PSDs of airborne SiO_2 nanoparticles were determined by AFM. The maximum particle height was chosen as the measurand for the particle size, and was supposed to be equal to the diameter d_a in the case of spherical particles. The height should be taken on the particle apex relative to the surrounding substrate surface. Two reference AFM samples were used to establish metrologic comparability: (1) a calibrated height standard, consisting of a grating with a calibrated step height and corresponding expanded uncertainty of 41.2 ± 0.7 nm, and (2) a reference particle sample composed of monodisperse spherical polystyrene latex particles (3050A, Thermo Fisher Scientific), with a mean diameter of 46 ± 2 nm certified by TEM. These reference samples were circulated to all participants for the purpose of calibrating their AFM and to provide a common reference for the comparison. One sample of each aerosols OP and DP, called M* and collected on mica plates, was circulated to three AFM laboratories (AFM1, 2, and 4) for comparison.

AFM measurement protocol Measurement method and AFM set-up were chosen according to the best practice used by the participants. The AFM resolution was chosen to give a corresponding pixel side length of approximately 4 nm, which led to a reasonable lateral resolution for a 25-nm particle. The resolution in the z direction was estimated to be better than 1 nm for all participants. A scan range of approximately 2×2 μm at a time was measured for an AFM image size of 512×512 pixels. Tapping or intermittent mode was preferred to scanning in contact mode, since particles on substrates were more easily detached by the AFM tip in contact mode. However, use of a soft cantilever could reduce this risk even during contact mode. Supersharp tips were recommended for better image resolution, but not required, since the measured particle height was largely independent of tip shape.

In order to allow a reasonable statistical evaluation of the PSD, a minimum of 400 measured particles per sample was recommended with a number of images based on the expected particle density. The set 1 reference grating with the step height of 41.2 nm was measured once. The scan range was set to 20 μm × 20 μm. The measured height of the step was determined according to ISO 5436 and reported together with the expanded uncertainty. The AFM parameters for each laboratory are given in Table 4 in Appendix.

AFM result treatment The heights of the measured particles (at least 400) in all images were recorded and each image was levelled to obtain a substrate surface parallel to the x–y plane. This could be accomplished by a first-order plane fit which was subtracted from the complete image. Ideally, only the substrate pixels were used for this levelling. The size of each particle was assessed by the height of the highest point of the particle. Further techniques such as line-wise levelling can be appropriate if the scanning is exposed to instrumental drift. Note that the line-wise levelling required a fit limited to the substrate pixels only, as many particle pixels per scan line might lead to a bias. As the reference surface was sufficiently flat with only little surface roughness, a second- or third-order model for the levelling could be considered by the involved laboratories.

AFM measurement uncertainty evaluation The measurement uncertainty was estimated by each participant according to their measurement methods, data processing, and the instruments implemented for the comparison. The measurement protocol used for the determination of the particle heights requires an estimation of the height level of the sample substrate that serves as a reference surface, as well as the measurement of the maximum height on each particle. Obviously, this method is very sensitive to the noise level along the z direction and to a larger extent also to the roughness of the samples. Concerning the latter point, freshly cleaved mica substrates possess an atomically flat surface with a very low roughness that can be neglected in the uncertainty budget. However, this is not the case for the grids or filters used to deposit the nanoparticles during most of the aerosol sampling experiments. For these substrates, the surface roughness becomes clearly the main contributor for the measurement uncertainty. Another significant source of uncertainty is related to the individual calibration of the different instruments with the transfer standard used during the comparison.

Scanning electron microscopy

After their generation and sampling on PMF substrates, PSD of the SiO_2 airborne nanoparticles were measured by SEM. Modern SEM operated with very finely focusable electron beams (such as cold field emission gun), or working at low electron beam voltages (so that electrical charging of insulating specimens becomes insignificant) or with electron detectors of higher sensitivity (such as "In-Lens" or "Through-the-Lens" detectors) can enable accurate analysis of nanoparticle sizes well below 100 nm. As presented in Table 5 in Appendix, a diverse range of SEM instrumentation was employed by the participants, but it is representative of the most commonly used microscopy techniques for the characterization of specimen surface morphology at the nanometre scale. As sources, electron guns such as tungsten (well-known for providing electron beams of poor resolution) and (cold or thermally assisted) field emitters (ensuring high resolution) were used. As detectors, both conventional Everhardt-Thornley (ET) and "In-Lens" and "Through-The-Lens" detectors were used.

Taking into account differences in instrumental performances between the microscopes used, only three relevant constraints were imposed: (1) accelerating voltage: a range of 1–30 kV was chosen. Depending on equipment, the high-resolution low-voltage operation mode was preferred to the conventional high-voltage mode, with the aim of avoiding electrical charging effects that necessitate coating with a thin conductive film; (2) a magnification between $250,000\times$ and $300,000\times$ was chosen. However, it was possible to choose another magnification between $50,000\times$ and $300,000\times$ depending on the individual constraints of laboratories to take images of about 500 or 1,000 nanoparticles; (3) the image magnification calibration was performed with nanoparticle CRMs having a mean diameter similar to those of the SiO_2 nanoparticles. Such CRMs of nanoparticles in aqueous suspensions were distributed by the SMPS4 lab to all participants: (i) Polystyrene Latex Spheres (PSL) with mean diameter of 81 ± 3 nm certified by TEM (3080A, Thermo Fisher Scientific), (ii) two reference materials of gold nanoparticles with mean diameters, measured using SEM, of 26.9 ± 0.1 nm and 54.9 ± 0.4 nm (RM 8012 and RM 8013, NIST) which did not require a conductive coating. Further useful instrumental parameters for each laboratory are given in Table 5.

Sample preparation for SEM analysis After particle collection on PMF and before SEM analysis, a thin film of Au, Ag, Pt, or Pd was sputter deposited in order to ensure an electrically conductive surface and to avoid surface charging under electron bombardment at high accelerating voltages. For laboratories equipped with a low-voltage microscope, the influence of the coating on particle size measurements was assessed. Both the PSL calibration and the airborne particle measurements (aerosol OP and DP) were performed under the same conditions to enable comparison of the measurement results with and without coating. This constitutes one way of estimating the measurement uncertainties due to the applied coating.

SEM measurement protocol In order to check the uniformity of the particle collection over the whole sample area, a preliminary survey of the PMF sample with the deposited nanoparticles was performed. It was determined that the average distance between neighbouring particles should not be shorter than their average diameter, in order to avoid overlaps which made the correct identification impossible.

For aerosol OP, about 500 particles were measured, while about 1,000 particles were measured for aerosol DP. It is important to avoid overlaps between the scanned areas of different SEM microphotographs and it was necessary for the scale bar to be visible on each microphotograph. If coating was used, a thickness correction including measurement uncertainties was applied.

SEM results treatment ImageJ software (Collins, 2007; Rasband 1997–2009) was used for processing and analysis of the SEM images. Other equivalent softwares (e.g. Image Pro Plus or functionality incorporated in the SEM software package) were used for particle image treatment (see Table 5). Particle diameter was defined as the mean length (L) and the width (l) of ellipses circumscribing particles (method used to determine the shape of the particle). For the ellipse as a circle case, only conventional diameter was determined. Other parameters such as perimeter and area were also given. The mean, mode, and standard deviation (SD) of the diameter distribution for each sample were then calculated. For the case of a bi-modal size distribution, the peak and the area ratios were also reported. Obvious imaging artefacts were eliminated manually.

SEM measurement uncertainty evaluation Contributions of the image magnification calibration uncertainty as well as of the coating thickness were taken into account for the evaluation of the measurement uncertainty. Selection of threshold in the greyscale images was of decisive importance for an accurate delimitation of the nanoparticles in the evaluation of the diameter measurement uncertainties. It is important to note that the data reduction software required the redefinition of the pixel size of each particular micrograph.

Methodology for TEM analysis

After the particle generation and sampling on TEM grids and PMF substrates, the particle size was measured by TEM. The TEM laboratories involved in the interlaboratory comparison used two types of instruments: (1) TEMs with thermo-ionic electron sources [tungsten (W) or lanthanum hexaboride (LaB_6) filaments] operated at 100 and 200 kV, (2) TEMs with Schottky-type field emission sources (FEG) operated at 200 and 300 kV. As seen in Table 6, the spatial resolution of all the involved instruments was at the same level, i.e. about 0.2 nm. Moreover, the laboratories performed imaging used the same imaging mode, i.e. bright field TEM (BFTEM). Digital BFTEM images were recorded on CCD cameras of with detectors ranging from 1,024 × 1,024 to 4,008 × 2,672 pixels.

TEM acquisition protocol Taking into account the difference between the involved microscopes types, three important parameters were imposed: (1) accelerating voltage: a range of 100–200 kV (depending on the equipment) was chosen; (2) magnification: the preferred magnification range was between 250,000× and 300,000×. However, imaging at differing magnifications (50,000× to 300,000×) was allowed depending on the laboratories constraints to perform the images of 500 or 1,000 nanoparticles; (3) TEM calibration was performed using CRMs. PSL CRMs were certified by TEM (46 ± 2 nm (3050A, Thermo Fisher Scientific), 81 ± 3 nm (3080A, Thermo Fisher Scientific)) in aqueous dispersion for direct deposition on TEM grids. Another RM was an aqueous dispersion of gold nanoparticles (RM 8012 and RM 8013, NIST; mean diameters, measured by TEM, equal to 27.6 ± 2.1 nm and 56.0 ± 0.5 nm, respectively). A third CRM was a gold grating replica on a copper TEM grid (2,160 lines/mm). All the acquisition parameters employed by the laboratories of the TEM interlaboratory comparison are presented in Table 6.

Sample preparation for TEM analysis For off-line TEM imaging, 200 mesh standard copper grids, covered with Formvar/carbon film and with carbon only, were chosen. Three methods for deposition of SiO_2 nanoparticles onto the grids were employed: (1) Type A sampling (direct sampling on TEM grid): SiO_2 nanoparticles were simultaneously deposited on PMF and on TEM grids placed beneath a membrane, (2) Type B sample (direct sampling on TEM grid): NAS sampling on one TEM grid, (3) Type C sampling (indirect sampling): nanoparticles were first deposited on a PMF from which they were transferred to TEM grids via its dissolution according to Sebastien et al. (1978), by the Environmental Protection Agency procedure (1987) and Spurny (1994).

After sampling, a piece of PMF was coated with a thin graphite film by vacuum evaporation, placed on TEM grid, and partially dissolved using $CHCl_3$ (ultrapure 99 %). In this way particles are sandwiched between PMF and evaporated graphite film. This dissolution was realized using: (i) a thermostatic bath at 55 °C for about 8 h, (ii) a petri dish at room temperature for about 24 h, (iii) a low vacuum for about 10 min. Sampling on TEM grids by each of the sampling techniques listed above are ready for further direct observation in TEM, i.e. without need of any additional preparation step. This is not exactly the case with the SEM imaging, which, depending on the type of SEM instrument employed, may require the application of a conductive coating to the as-sampled specimens.

TEM measurement protocol A preliminary scanning of the entire grid was performed in order to check the particle distribution and the collection uniformity. As with the SEM measurement protocol, the average distance between neighbouring particles should not be shorter than their average diameter to avoid overlaps. Since expected size distribution of nanoparticles was in a range between 20 and 100 nm, magnifications of 50,000× to 300,000× were recommended. For aerosol OP, about 500 particles were measured while about 1,000 particles were measured for aerosol DP. It was important to prevent overlaps between the scanned areas of different TEM microphotographs and it was necessary that the scale bar be visible on

each microphotograph recorded in at least ten random 90×90 µm squares of the grid.

TEM results treatment The result treatment of TEM were identical than the SEM result treatment (see "Scanning electron microscopy").

TEM measurement uncertainty evaluation Calibration of image magnification and the TEM grid mounting (the sampling side mounted towards the electron gun) were taken into account for the measurement uncertainty. To ensure correct grid orientation, each grid box sent to participants contained clear identification of the mounting side of TEM grids. An additional post-acquisition uncertainty that originated from the diameter measurement uncertainty, which depended on the accuracy of thresholding to digital greyscale TEM images, was also included.

Results and discussions of inter-laboratory comparison

On-line measurements

Figure 3 shows two examples of PSD results plotted as a function of the logarithmic electrical mobility diameter of airborne particles, for aerosols OP (left side) and DP (right side). The y-axis ($dM/d\log(d_{m})$) represents the number concentration of the collected particles divided by the width (in logarithmic scale) of different channels of the diameter measurement. The mean and mode diameter values of size distributions with the different associated uncertainties (σ_R

standard deviation of reproducibility, u combined standard measurement uncertainty and U expanded uncertainty with the coverage factor $k = 2$), obtained by the different participants for aerosols OP and DP in this inter-laboratory comparison, are presented in Tables 7 and 8 in Appendix.

For aerosol OP, the standard deviations for repeatability and reproducibility are less than or equal to 1 nm and the expanded uncertainties below 4 nm. Different diameter ranges were investigated to determine the mean diameter. The first range is close to the peak in order to decrease the influence of the different artefacts due to impurity particles created during the generation (fine particles below 20 nm) and/or doublet particles. The second range corresponds to the total DMA range in order to detect all produced particles.

The aerosol generation systems used (atomizer and electrospray) were optimized in order to produce primary SiO_2 particles without agglomeration.

Most of the mean diameters obtained by all laboratories for the aerosol OP (Table 7), with different operating modes and data analysis, lie between 32 and 36 nm, except for results from laboratory SMPS3 (mean diameter of 43 nm). The mode diameters are between 35 and 37 nm. The values of the mode diameter do not change for different choices of the size ranges and the statistics laws. Results from laboratory SMPS4 are presented in Table 7 for aerosol OP (scanning 1 and 2) and show that the different ranges used to determine the mean diameter lead to a difference of only 2 nm with an atomizer system. This difference was reduced to 0.6 nm with an electrospray system, obtained by laboratory SMPS5 for two different ranges and two different operating conditions (scanning and stepping). A
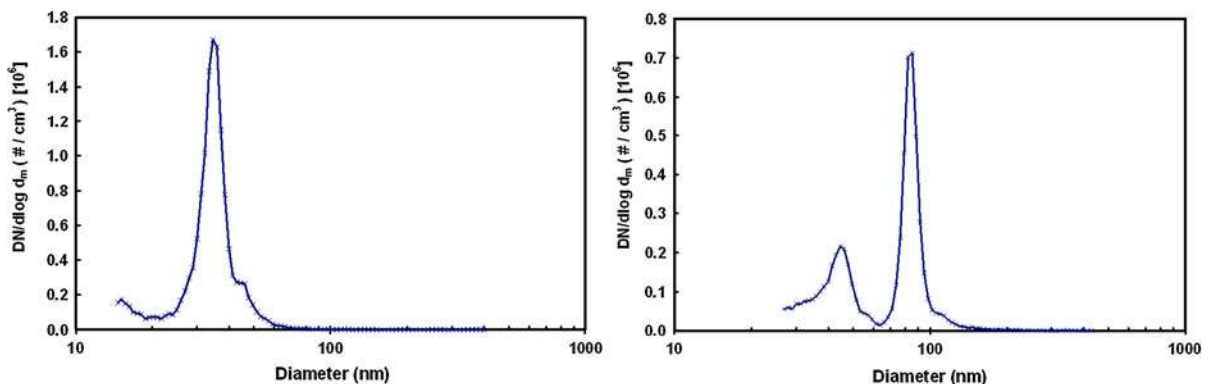

Fig. 3 Examples of size number distribution obtained using the generation setup and SMPS size characterization of SiO_2 airborne nanoparticules for aerosols OP (*left side*) and DP (*right side*)

difference of 2 nm is also obtained by laboratory SMPS2 if a Gaussian law is used rather than the mean diameter given by the AIM software.

Table 8 presents the results obtained for the mean and mode diameters for both aerosol DP populations (the minor and major population, respectively). The peak and area ratios of these two populations are also presented. Most of the standard deviations for repeatability and reproducibility are below 1 and 0.6 nm for the first and the second populations, respectively. Only the repeatability and reproducibility standard deviations obtained by laboratory SMPS3 for the mode diameter of the first population are higher (5 and 6 nm, respectively). The expanded uncertainties are, respectively, below 13 and 4 nm for first and the second populations. For the first and second populations, the mean and mode diameters obtained by all laboratories, with different operating modes and data analysis, are comprised between 39 and 46 nm, and between 82 and 88 nm, respectively. Some results, such as those for laboratory SMPS4, show that the range used to calculate the statistic diameters with the same data could lead to a difference of 5 nm for the mean diameter; no difference was observed for the mode diameter. The results show that the operating modes (stepping or scanning) with two different ranges lead to a difference of 2 nm for mean and mode diameters of the first population, and to 4 nm for the mode of the second population. The peak ratios (peak intensity obtained for the mode of the first population divided by peak intensity obtained for the mode of the second population in %) are mostly between 16 and 21 %, except for the ratios from laboratories SMPS1 and SMPS3, with 52 and 40 %, respectively. The area ratios (ratio in particle number concentration between the first and the second populations in %) are slightly higher than the peak ratios with results between 18 and 63 %. The smallest ratio is obtained by laboratory SMPS5 using electrospray as a generation system. This could be due to a reduction of the number of residual and agglomerated particles with electrospray, compared to atomizer generation.

Figure 4a, b presents, respectively, the measured aerosol OP and aerosol DP mean diameters. The total average mean and mode diameters with ±two interlaboratory standard deviations are 35.1 ± 6.4 nm and 35.4 ± 2.0 nm for aerosol OP, 44.0 ± 4.0 nm and 44.2 ± 5.3 nm for the first aerosol DP population; and 85.0 ± 4.1 nm and 83.1 ± 3.4 nm for the second aerosol DP population (Tables 1, 2). The results of mean and mode diameters are included in the intervals of the associated two interlaboratory standard deviations (Fig. 4a, b; Tables 7, 8), except for the mean diameter OP from laboratory SMPS3.

A significant effort was made to produce a stringent common protocol, both for aerosol generation and for SMPS measurements. However, differences remain between laboratories for the aerosol generation and measurement equipment and conditions such as CPC choice, DMA flow conditions, data processing, and also diffusion and charge corrections. Therefore, the low standard deviations of repeatability and reproducibility, obtained for each laboratory, show some variation in the results due to differences between the applied protocols. Concerning the scanning mode operation, the influence of different aerosol generators, DMA flow conditions, and the presence or absence of diffusion and charge corrections were investigated to evaluate measurement uncertainty components and to calculate the expanded uncertainty. All laboratories results (mean and mode diameters) for aerosol OP and DP, except for the mean diameter OP from laboratory SMPS3, are in agreement with each other using the combined standard measurement uncertainty, and in even better agreement using the expanded uncertainty with the coverage factor $k = 2$ (Tables 7, 8).

The repeatability/reproducibility and measurement uncertainties obtained in stepping mode operation by laboratory SMPS5 are smaller than those for the scanning mode (Tables 7, 8). The stepping mode expanded uncertainties were evaluated by taking into account other uncertainty sources such as reference particle diameters, DMA voltages, slip correction, and fitting function choices, charge correction and Brownian motion effects. The results obtained by stepping mode with an electrospray generator, which integrates a correction using the reference particle diameter (CRM), are in good agreement with scanning mode and correspond to a more accurate value.

Off-line measurements

Atomic force microscopy

The diameter of the nanoparticles was determined by their apex heights above the substrate surface, assuming spherical nanoparticles. The diameters of the airborne nanoparticles were measured on four different substrates by four participants (Fig. 4c; Table 9 in Appendix) for the aerosol OP and by three participants for the

aerosol DP (Fig. 4d; Table 10 in Appendix). Tables 9 and 10 in Appendix present the mean and mode diameters values, the standard deviation of the obtained PSDs for the different labs for aerosols OP and DP with the different associated uncertainties. The same sample on a mica substrate, indicated by "M*", performed by laboratory SMPS4 (Tables 9, 10), was measured by laboratories AFM1, 2, and 4.

Typically, 100–500 particles were measured by each participant. For aerosol OP, good metrological compatibility of the participant results is shown.

Most of the mean diameters for the aerosol OP are comprised between 27 and 33 nm (cf. Fig. 4c), except for result from laboratory AFM4 (mean diameter of 35 nm). The mode diameters are between 27 and 33 nm (Table 9 in Appendix). The expanded uncertainties associated to mean and mode diameters for aerosol OP are below 7 nm. For the first and second aerosol DP populations, the mean diameters are, respectively, comprised between 32–42 nm and 78–85 nm (cf Fig. 4d). Concerning the aerosol DP mode diameters, the results are comprised between 36–45 nm and
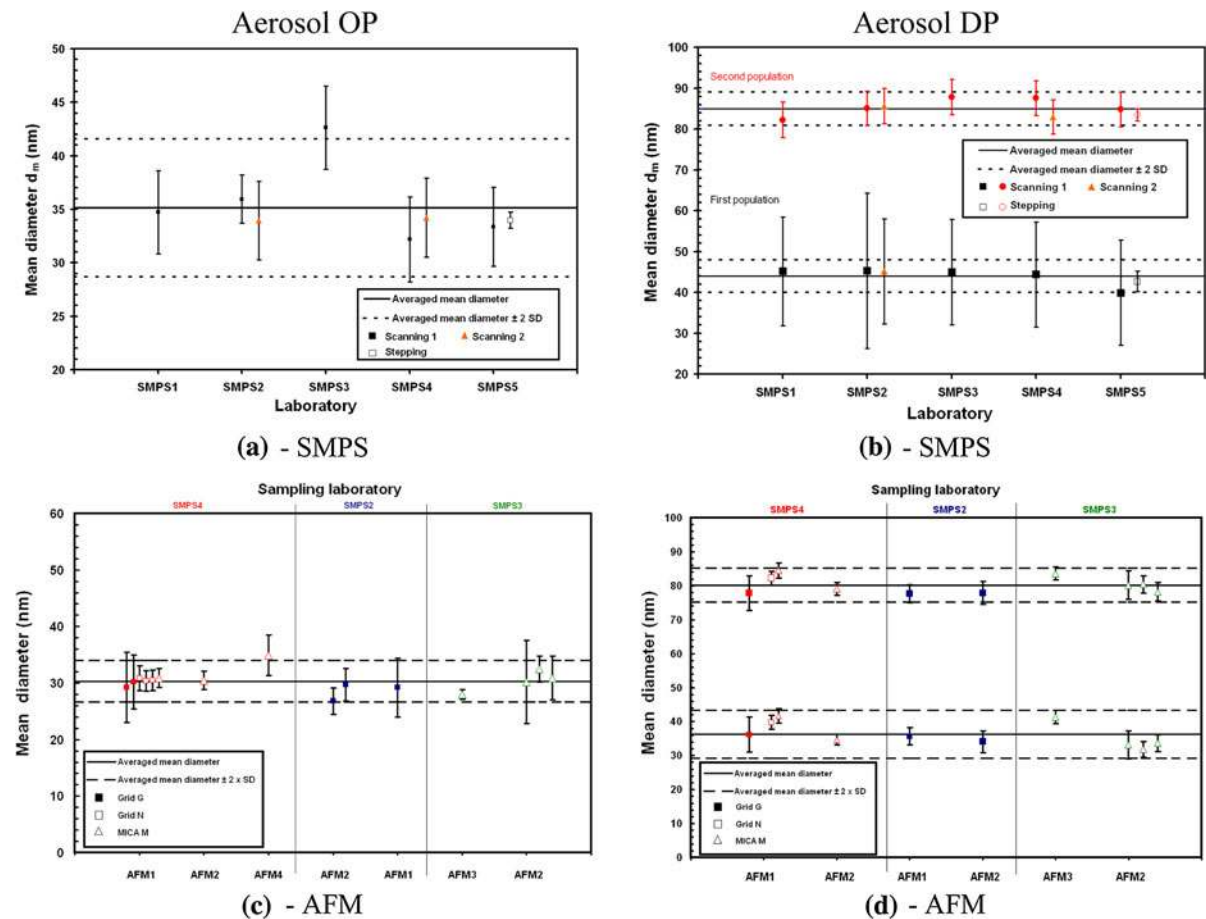
Fig. 4 SMPS measurement results for aerosol OP (**a**) and aerosol DP (**b**) mean diameters. AFM measurement results of the mean diameters of aerosols OP (**c**) and DP (**d**) samples for various substrates and samples of each measurement laboratory associated with the sampling laboratory (SMPS2, SMPS3, and SMPS4). *Filled* and *empty squares* represent the G and N grids, respectively. *Triangles* represent samples on mica substrates. SEM results of the measurement of the mean diameters for aerosols OP (**e**) and DP (**f**) samples of each measurement laboratory associated with the sampling laboratory (SMPS2, SMPS3, and SMPS4). *Filled* and *empty squares* represent measurements with and without coating, respectively. TEM measurement results of the mean diameters of aerosols OP (**g**) and DP (**h**) for various samples of each measurement laboratory associated with the sampling laboratory (SMPS1, SMPS2, SMPS3, and SMPS4). *Filled* and *empty squares* represent the G and N grids, respectively. *Empty triangles* represent the "g" grids transferred from a PMF sample to grids. *Error bars* indicate the expanded uncertainty ($k = 2$). The *solid line* represents the total average within a band of ±two interlaboratory standard deviations (*dashed lines*)

Aerosol OP

(e) - SEM

(g) - TEM

Aerosol DP

(f) - SEM

(h) - TEM
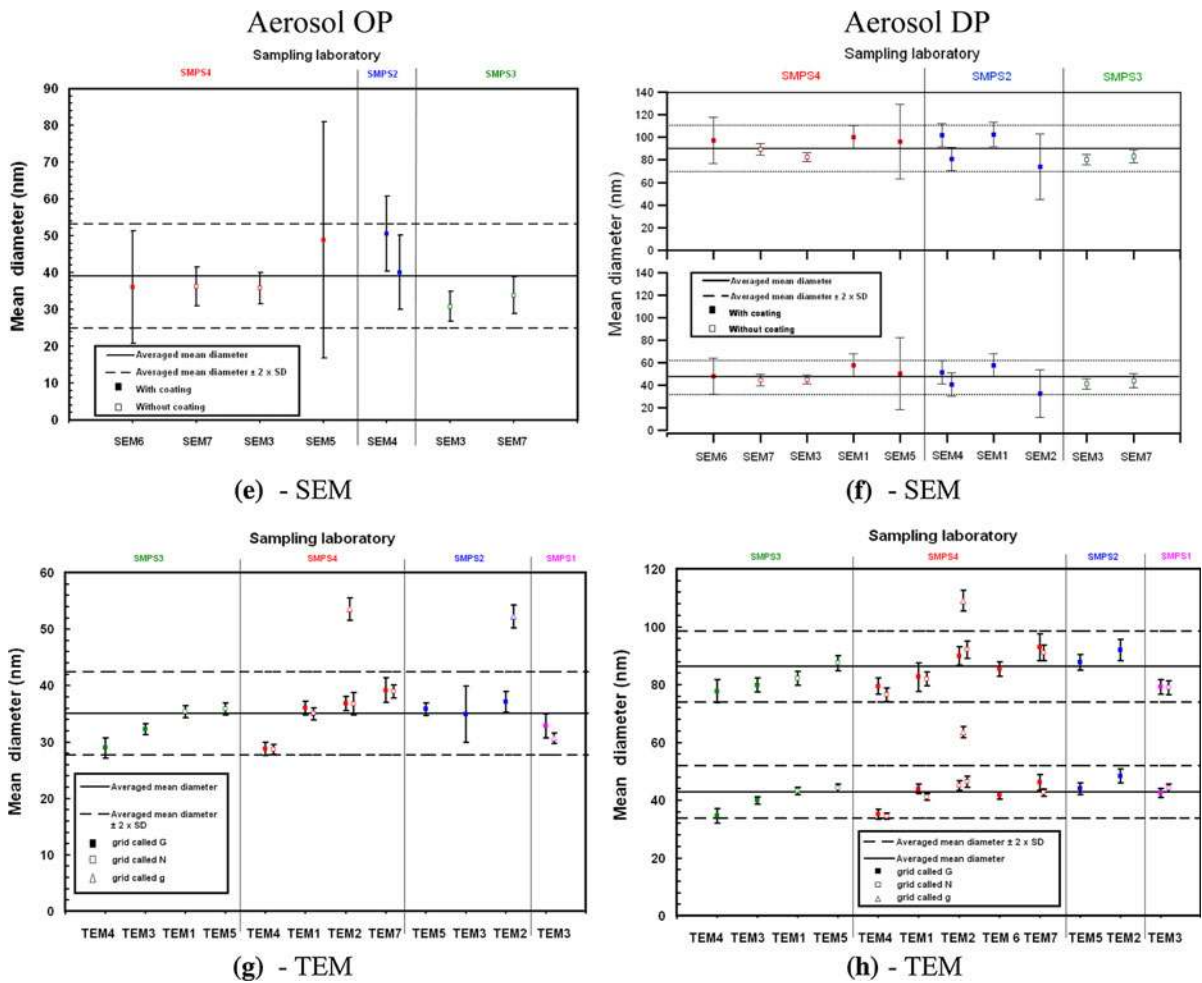
Fig. 4 continued

Table 1 Average mean and mode diameter of aerosol OP. SD corresponds to the calculated standard deviations of the average measurements of all SMPS, SEM, TEM, and AFM laboratories involved in this interlaboratory comparison

	Averaged mean diameter d_p (nm)	$2 \times$ SD (nm)	Averaged mode diameter d_p (nm)	$2 \times$ SD (nm)
SMPS	35.1	6.4	35.4	2.0
TEM	35.1	7.4	35.6	7.6
SEM	39.0	14.2	38.3	14.1
AFM	30.3	3.7	30.4	5.1

78–86 nm. The expanded uncertainties of both statistic diameters for the first and second populations are below 5 nm. AFM results for aerosols OP and DP show a good agreement between all laboratories. The mean and mode diameters with its associated expanded uncertainties are comprised in the band represented by the average with ±two interlaboratory standard deviations,

i.e. 30.3 ± 3.7 nm and 30.4 ± 5.1 nm for OP aerosol. In the case of aerosol DP, these diameters are also comprised in the average bands with ±two interlaboratory standard deviations, i.e. 36.2 ± 7.1 nm and 39.2 ± 6.8 nm for the first population and 80.2 ± 5.0 nm and 81.0 ± 5.3 nm for the second one, respectively (Fig. 4a, b; Tables 9, 10 in Appendix).

Table 2 Average mean and mode diameter of both populations of the DP aerosol

	First population				Second population			
	Averaged mean diameter d_p (nm)	$2 \times$ SD (nm)	Averaged mode diameter d_p (nm)	$2 \times$ SD (nm)	Averaged mean diameter d_p (nm)	$2 \times$ SD (nm)	Averaged mode diameter d_p (nm)	$2 \times$ SD (nm)
SMPS	44.0	4.0	44.2	5.3	85.0	4.1	83.1	3.4
TEM	42.9	9.0	43.7	11.9	86.3	12.3	88.1	12.0
SEM	46.6	15.1	47.0	13.8	89.8	20.4	91.1	19.8
AFM	36.2	7.1	39.2	6.8	80.2	5.0	81.0	5.3

SD corresponds to the calculated standard deviations of the average measurements of all SMPS, SEM, TEM, and AFM laboratories involved in this interlaboratory comparison

No significant difference was observed between the NAS grid samples: sample B, NAS mica (sample D), and the grid deposited on PMF (sample A). In general, a cleaved mica substrate provides an ideal, atomically flat reference surface for the measurement of particle diameters. We observed that the smallest measurement uncertainties of the mean particle diameters were obtained with the mica. Other substrates, such as grids or filters, show RMS surface roughness between approximately 1 and 10 nm. These roughness values have a significant impact on the measurement uncertainties. The expanded uncertainties can become as large as the 95 % percentile of the distribution of measured mean values, or even exceed it. The variations of peak and area ratios between both populations for the aerosol DP were mainly between 25 and 80 %, except for one measurement.

Scanning electron microscopy

Most commercial sputter coaters suggest coating thickness values which shall be reached when the coating applied runs under well-defined, recommended controlled conditions. Nevertheless, it was also stated that these given thickness values are rough estimates, so that a calibration of an accompanying witness specimen (silicon wafer) and separate traceable measurement of the coating thickness must be undertaken.

When the low-sputtering mode was used, the coating mean grain size reached typically about 2 nm for Au and about 1.7 nm for Au/Pd. The resulting well-known, irregular cauliflower-like structure is clearly visible in Fig. 5 (left) compared to uncoated samples Fig. 5 (right). The particle coating thickness was not necessarily the same as the one obtained on a flat surface. Therefore, accurate determination of the applied coating layer thickness was a challenging task which generated the most significant uncertainty contribution to the size measurement that may even exceed 10 nm.

The data reduction by image processing consisted firstly of the accurate "takeover" of the calibrated magnification, i.e. of the pixel size, associated with every individual SEM micrograph. Depending on the image processing software employed, the most significant part involving propagation into the measurement
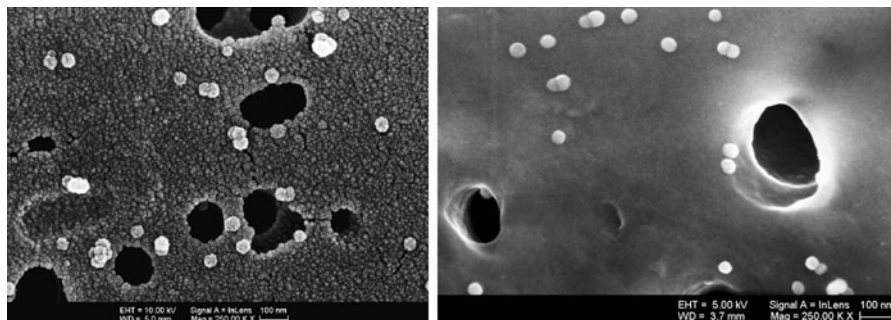

Fig. 5 SEM micrographs of aerosol OP specimen of type C (PMF as a support): coated with 10 nm Au (*left*); note the "cauliflower-like structure" of the Au coating altering the real size of the nanoparticles, and uncoated specimen sampled by the same laboratory in the low-beam voltage mode (*right*)

uncertainty was setting the threshold for the particle delimitation. No unique procedure was recommended in the present study but it was noted that the higher the quality of the acquired SEM micrograph was, the lower the uncertainty associated with the threshold setting becomes. In other words, it was highly recommended to invest the time to obtain a high-quality SEM micrograph. On the other hand, artefacts such as a slight oversaturation of the signals acquired with an In-Lens detector were observed by the participants. This contributes to an overestimation of the particle size. It was established that the particular mathematical/software procedures employed for determining the particle size (such as binarization or application of a "despeckle" algorithm for removing noise) may also lead to significant measurement uncertainty contributions. The "safest" way to get a realistic setting of the threshold is to simulate (by Monte-Carlo methods) SEM images similar to those which have been measured and to derive the corresponding particles size. Such pioneering work is challenging, but was recently successfully performed by Buhr et al. (2009).

Agglomerates of two or more nanoparticles or artefacts/defects of the support membrane were manually removed by some laboratories. Due to the coating applied by most of participants, it was realized that the image contrast caused by the pronounced surface morphology is quite similar to that of the nanoparticles sampled on PMF. Additional filtering (-out) options of the image processing software had to be taken into consideration, resulting in an increase of

the particle size measurement uncertainty. All the image processing steps together could induce uncertainties in determination of nanoparticle size of a few nanometers. Poorly acquired images (due to low performance instrumentation or an operator fault) lead to unacceptable size measurement uncertainty. The best supporting evidence constitutes the fact that only some participants could observe the aerosol OP specimens. However, with respect to the metrological purposes of the present study, they could not be resolved, i.e. no values are given in the Table 11 in Appendix. But the populations belonging to aerosol DP specimen could be resolved by all the participants.

Figure 6 shows a typical SEM micrograph taken during the intercomparison with the most important sequence in data reduction, namely the setting of the threshold. The SEM results obtained from all SEM laboratories are presented in the overview Tables 11 and 12 for aerosols OP and DP with the associated uncertainties.

The SEM results are in quite good agreement for the mode and mean values for both aerosol types. A second result is the good reproducibility of the values obtained by each laboratory. Standard deviations exceeding 10 nm were calculated only in the case of one laboratory, and no significant differences were found. The main sources of uncertainties discussed in the uncertainty section ("Scanning electron microscopy" section) range from 4 to 32 nm. Naturally, the smallest associated uncertainties of only 4–5 nm are those given by the laboratories having not necessarily applied a coating in order to measure without surface
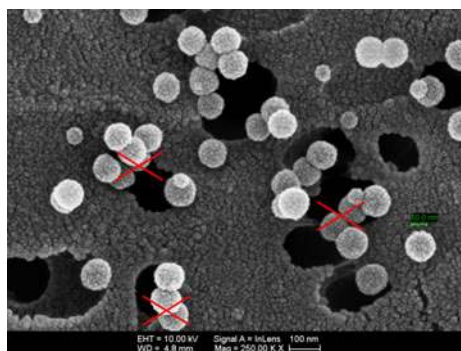
Fig. 6 SEM micrograph example for aerosol DP sample of type C coated with about 10 nm Au (*left*) and image processed after pixel calibration with ImageJ software (*right*). Most touching particles have been eliminated manually from the data reduction (see the *red crosses*). One should note that this example is a
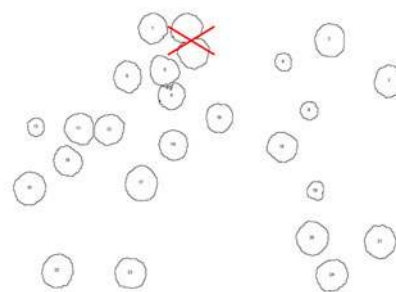
rather unfavourable one due to the relative large fraction of touching particles, however, it was deliberately chosen in order to illustrate the "manual" intervention during image processing. An automatic image processing would have produced significantly worse results

charging. The large uncertainty value of 32 nm was from a particular laboratory which had not corrected at all for the coating thickness. The reproducibility of the laboratory results, corresponding to twice standard deviation, was calculated from measuring the same set of three different samples SMPS laboratory sampling. In the case of the measurement without coating, 2SD reproducibility differences between the mean diameters do not exceed 2 nm for the nanoparticle population of lower size, and below 4 nm for the case of the population of nanoparticles of larger size. The associated uncertainty expressed as the double standard deviation ranges from one-third of the mean value for the two populations with quite similar, smaller size, to about a fifth of the mean value of the population with the larger size.

Seven measurement laboratories were involved in the SEM analysis. Figure 4e, f shows the measured mean diameter values, with expanded uncertainties ($k = 2$), for aerosols OP and DP. The PMF sample (sample C) was analyzed as coated and uncoated aerosol particles (filled and empty squares, Fig. 4e, f). Concerning the diameter measured from the coated sample, laboratories SEM4 and 5 did not take into account a correction factor for coating thickness, but included this correction in the uncertainty calculation. Only laboratory SEM6 applied a correction of 20 nm for the mean and mode diameters of both aerosols OP and DP, while laboratories SEM1 and 2 applied a correction of 5 and 26 nm, respectively, for aerosol DP mean and mode diameters. The expanded uncertainty was calculated as the root mean square of the square sum of SD reproducibility and an uncertainty which depends on several instrumental parameters such as magnification calibration, coating thickness and pixel calibration/threshold image selection. The reproducibility alone cannot explain the interlaboratory result differences (cf. Tables 11, 12), however, taking into account the expanded uncertainty, the laboratory results are in agreement. For aerosol OP, mean and mode total average diameters within a band of ±two interlaboratory standard deviations are 39.0 ± 14.2 nm and 38.3 ± 14.1 nm, respectively (Fig. 4e; Table 1). For aerosol DP, these values are, respectively, 46.6 ± 15.1 nm and 47.0 ± 13.8 nm for the first population and 89.8 ± 20.4 nm and 91.0 ± 19.8 nm for the second one (Fig. 4f; Table 2). The two interlaboratory standard deviations were higher compared to the other techniques (SMPS, TEM, and AFM)

due to the measurement results with and without coating, and mainly due to values without correction of coating.

For example, laboratory SEM3 determined a mean diameter with an expanded uncertainty ($k = 2$) of 45.1 ± 4.2 nm and 82.5 ± 4.1 nm for the first and second population of aerosol DP without coating, respectively. These values can be compared to the corresponding results from laboratory SEM7 which are 43.8 ± 6.1 nm and 83.2 ± 5.6 nm. Higher differences were obtained by laboratory SEM1 (57.6 ± 10.1 nm and 100.3 ± 10.2 nm), where PMF samples were Pt coated by taking into account a correction of 5 nm. For aerosol DP, peak and area ratios between first and second population maximum intensities were calculated for each measurement. These peak ratios vary between 15 and 62 % and a similar variation for the area ratios was obtained between 10 and 59 %.

Transmission electron microscopy

Proper mounting of a grid, the optimized usage of CCD camera dynamic range in TEM digital imaging, and the effect of objective aperture on BF TEM image of silica NPs were considered due to their influence on the imaging procedure. The grid should be oriented with its "face" surface towards the electron source. This fact was specifically stressed in the measurement protocol and was found to have sufficient effect on final size values calculated from TEM BF images. Adjustment of contrast/brightness parameters for the recording device (CCD camera) provides optimal usage of the whole matrix of the CCD camera and eliminates "dead pixels" (where information is lost because of under- or oversaturation). It is also well-known that under the smaller objective aperture the BF TEM image acquires stronger contrast. Therefore acquisition of BF TEM images with objective aperture inserted was recommended.

Numerical data about sizing of silica nanoparticles were obtained via post-acquisition processing of digital BF TEM images. The true geometry of nanoparticles was found to be imperfect (Fig. 7a, b), i.e. observed deviations from spherical morphology were pronounced enough to render the recommended circumscribing with an ellipse inaccurate. In addition, automated particle delimitation based on grey level threshold was found to be not accurate enough.

Seven measurement laboratories participated in the TEM interlaboratory comparison study, each with
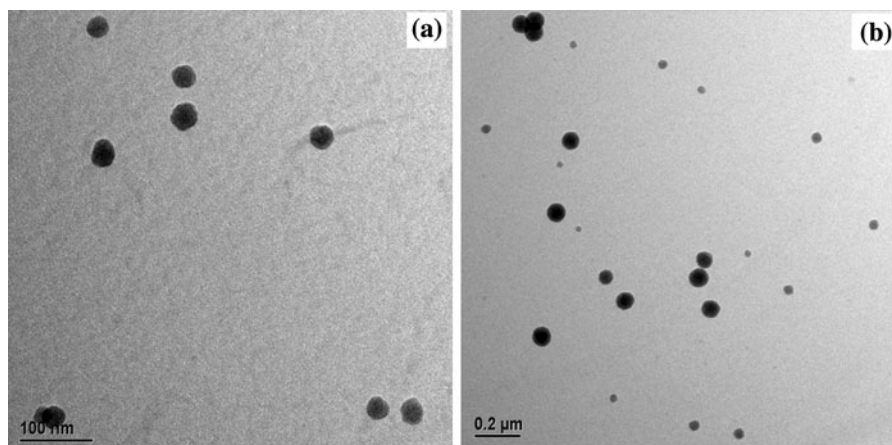
Fig. 7 BF TEM images for **a** aerosol OP and **b** aerosol DP

different instrument specifications and methods for processing the measurement data. For the calibration procedures used by the participants of this interlaboratory comparison (Table 6 in Appendix) a larger uncertainty of about 3 % was taken into account. The expanded uncertainty was calculated as the root mean square of the square sum of SD reproducibility of each laboratory and the uncertainty component of about 3 %. Results of TEM based on size measurement of aerosol OP and DP are presented in Tables 13 and 14 in Appendix.

Figure 4g presents the mean diameter values obtained by TEM laboratories for the aerosol OP. In the same way, Figure 4h presents aerosol DP measurements. The results showed that mode and mean diameter values were very close, without taking into account the diameters obtained from grid "g" measurements. The expanded uncertainties associated to mean diameters for aerosols OP and DP are below 5 nm.

For aerosol OP, the total average of mode and mean diameters within a band of ±two interlaboratory standard deviations are 35.6 ± 7.6 nm and 35.1 ± 7.4 nm, respectively (solid and dotted lines, Fig. 4h; Table 1). Mode and mean total average diameters are, respectively, 43.7 ± 11.9 nm and 42.9 ± 9.0 nm for the first aerosol DP population, and 88.1 ± 12.0 nm and 86.3 ± 12.3 nm for the second population (Table 2). These total averages were calculated without taking into account the diameters obtained from grid "g" measurements, i.e. the nanoparticles transferred from a PMF sample to grids, since a significant

difference was obtained for the diameter measurement results in this case. For example, laboratory SMPS4 obtained an averaged mean diameter of 53.6 ± 1.2 nm for aerosol OP from grid "g1" measurements (empty triangles, Fig. 4g), while a value of 36.8 ± 0.6 nm was obtained from measurements on grid "G1" performed on the same sample A, i.e. a difference of about 16.8 nm between the two measurement types. Similar differences were observed for aerosol DP. Therefore, a transfer of NPs initially deposited on nucleopore membrane onto a TEM grid may increase their size by 50 % for the aerosol OP of the first aerosol DP population and 25 % for the second aerosol DP population. This increase seems to occur due to the evaporated graphite film and the chloroform dissolution used during the transfer of NPs on nucleopore membrane onto a TEM grid. However, no significant difference was observed between measurements of samples B (TEM grid + NAS sampling) and A (grids on PMF sample). This can be seen in Fig. 4f, g by comparing filled and empty squares (grids G and N, respectively) for a specific sampling laboratory. For example, the average mean and mode diameters of 36.8 ± 0.6 nm and 37.3 ± 0.3 nm obtained by laboratory TEM2 for sample A (grid G) produced by the SMPS 4 sampling laboratory are very close to the values of 36.8 ± 1.6 nm and 37.3 ± 1.8 nm measured for sample B (grid N) for aerosol OP. Similarly, no significant differences of the measured diameter values were observed between G1 and G2 grids, i.e., between carbon-coated Formvar film and pure carbon film on 200 mesh Cu grids.

Summary, recommendation, and outlooks

In this work, two different silica nano-aerosols were generated and studied by on-line and off-line techniques: one contained a single population of nanoparticles, and the second one composed by two populations of non-agglomerated nanoparticles. This study describes the methodology (sampling, sample preparation, measurement protocol, operating parameters, treatment of the results, traceability, and calibration) and presents results obtained with an evaluation of the measurement uncertainty. Metrologically traceable size measurements provided reliable PSDs results for SiO_2 airborne nanoparticles.

Some methods were proposed to generate aerosols and to measure their PSDs by SMPS, describing the operating parameters, metrological traceability, calibration of the spectrometers for the purpose of size measurement, evaluation of the measurement uncertainty, and treatment of the obtained results. Five SMPS laboratories were involved in this study and obtained on-line measurement results in good agreement taking into account the expanded measurement uncertainty. The total average ± two interlaboratory standard laboratory deviations (SDs) for the mean and mode electrical mobility diameters were 35.1 ± 6.4 nm and 35.4 ± 2.0 nm, respectively, for aerosol OP, 44.0 ± 4.0 nm and 44.2 ± 5.3 nm for the first aerosol DP population; 85.0 ± 4.1 nm and 83.1 ± 3.4 nm for the second one. The geometric SD or SD of the measured size distribution showed that the population of aerosol OP and both populations of aerosol DP, taken separately, were monodispersed. Consistent SMPS results allowed validation of the on-line measurement methodology proposed for the size distribution in case of both studied nano-aerosols. For aerosol DP, peak and area ratios were mainly determined between 20 and 60 %.

Concerning off-line measurements, different protocols were proposed for the sampling (filtration and electrostatic precipitation) onto different substrates (carbon-coated Formvar film and pure carbon film Cu grids, PMFs, and mica substrate). Different sampling methods and sample preparation (e.g. the use of conductive coatings for the SEM samples, the transfer of particles from PMF to TEM grids) on the measured PSDs for aerosols OP and DP were discussed. A protocol for storage conditions and sample transport was proposed in order to avoid positive and negative artefacts of the PSD and to prevent air pollution.

Seven laboratories were involved in the TEM analysis, seven in SEM, and four in AFM measurements in order to compare mean and mode diameters obtained by these techniques from aerosol deposited on grids, filters, and mica plates by an electrostatic precipitation and filtration technique using SMPS controlled generation upstream.

For aerosols OP and DP, AFM results were consistent among the four participants within their measurement uncertainties. Total mean and mode diameters for aerosol OP were determined to be 30.3 ± 3.7 nm and 30.4 ± 5.1 nm, respectively. For aerosol DP, same diameters were equal to 36.2 ± 7.1 nm and 80.2 ± 5.0 nm for the first population and 39.2 ± 6.8 nm and 81.0 ± 5.3 nm for the second population (cf. Tables 1, 2). No significant difference was observed between the different samples of NAS grid (sample B), NAS Mica (sample D), and grid deposited on PMF (sample A). A cleaved mica substrate provided an ideal, atomically flat reference surface for the measurement of particle heights. Not surprisingly, the measurement uncertainties for mean particle heights on mica are the smallest. The other substrates (grids or filters) showed RMS surface roughness between approximately 1 and 10 nm, with a significant impact on the measurement uncertainties. The uncertainties can become as large as the 95 % percentile of the distribution of all measured mean values, or even exceed it. The SDs of PSDs obtained by AFM were mainly between 3 and 9 nm for both aerosols OP and DP. The peak and area ratios of the two populations of DP aerosol varied mainly between 25 and 80 %.

We do not recommend the application of a conductive coating for the SEM measurement since it significantly affects the measured PSD. For example, a mean diameter of 5–26 nm without correction for aerosols OP and DP was obtained. If a coating was used, it was necessary to correct the diameter by a study of the coating effect and/or include the effect of the coating in the uncertainty calculation. We observed that the expanded uncertainty is significantly higher if the coating treatment was used compared to measurements without coating. For aerosol OP, mean and mode total average diameters with ±two interlaboratory SDs were 39.0 ± 14.2 nm and 38.3 ± 14.1 nm, respectively (cf. Table 1). For aerosol DP, these values were 46.6 ± 15.1 nm and 47.0 ± 13.8 nm, respectively, for the first population and 89.8 ± 20.4 nm and 91.0 ± 19.8 nm for the second population (cf. Table 2). The variation of peak and area ratio between the two

populations for aerosol DP was similar to the SMPS measurements, i.e. between 10 and 60 %. The SDs of PSDs obtained by SEM were mainly comprised between 4 and 9 nm for the populations of aerosols OP and DP.

The SEM reproducibility global SD was higher compared to the other techniques (SMPS, TEM, and AFM) since all measurements (with and without coating) were taken into account and were mainly due to the values without coating correction. The reference nanoparticles, from certified reference materials, played a relevant role in the analysis and were sampled, with a measurement protocol including calibration of the image magnification. However, several SEM measurements did not allow obtaining traceable results for nano-aerosol OP due to the lower performances of some SEM instruments. Nevertheless, modern instruments successfully analyzed all the sample types used in this interlaboratory comparison. The present study clearly proves that traceable measurements of aerosol nanoparticles size can be performed if sample preparation, instruments conditions, and SEM operator follow a strict measurement protocol as given in this paper.

The seven TEM laboratories involved in the comparison of aerosol OP particle sizes obtained mode and mean total average diameters with ±two interlaboratory SDs of 35.6 ± 7.6 nm and 35.1 ± 7.4 nm, respectively (cf. Table 1). Mode and mean total average diameters are, respectively, 43.7 ± 11.9 nm and 42.9 ± 9.0 nm for the first aerosol DP population, and 88.1 ± 12.0 nm and 86.3 ± 12.3 nm for the second population (cf. Table 2). These total averages were calculated without taking into account the diameters obtained from measurements on grid "g", i.e. the nanoparticle transfer from a PMF sample to grids, since a significant difference was obtained for the diameter measurement in this case. No significant differences in the obtained PSD were found between measurements for B (TEM grid + NAS sampling) and A (grids on PMF sample) samples. Similarly, no significant differences in the measured diameters were observed between carbon-coated Formvar film and pure carbon film on 200 mesh Cu grids, respectively.

Concerning the TEM sample preparation, we recommend direct deposition of nanoparticles onto a supporting TEM grid for accurate measurements of nanoparticles size in TEM. It was found that, unlike direct deposition on a standard coated TEM copper grid, a transfer of nanoparticles initially deposited on a nucleopore membrane onto a TEM grid may increase their measured size up to about 20 nm for the mean and mode diameter. This corresponds to the increase of the measured size by 50 % for the first aerosol DP population and by 25 % for the second aerosol DP population. The SDs of the PSDs obtained by TEM were mainly between 2 and 9 nm for the populations of aerosols OP and DP.

A major contribution to the TEM results uncertainty was due to post-acquisition image processing. By taking into account this expanded uncertainty, measurements were mainly consistent without consideration of measurements obtained by the transfer method.

For the simple shape (spherical) airborne nanoparticles, the different mode and mean diameters measurements by SMPS, AFM, SEM, and TEM were consistent considering the obtained standard deviation (cf. Tables 1, 2), even though the values for AFM were always slightly lower than those obtained using the other techniques. It is important to stress that we compared different equivalent diameters, namely the height diameter for AFM measurement, electrical mobility diameter for SMPS measurement, and geometric diameter for SEM and TEM measurements. The protocols proposed in this work will be used to provide international harmonized methodologies for the characterization of airborne SiO_2 nanoparticles.

Appendix

See Tables 3, 4, 5, 6, 7, 8, 9, 10, 11, 12, 13, and 14.

Table 3 Operating parameters of on-line measurement systems used by each laboratory in the interlaboratory comparison

Lab	Type of aerosol generator (manufacturer)	Types of DMA and neutraliser (manufacturer)	Impactor nozzle size (manufacturer)	Type of CPC (manufacturer)	DMA Voltage operation (time of operation)	Sheath flow (L/min)	Sample flow (L/min)	Analytical and corrections methods	Traceability	Calibration (difference between Certified value of CRM and experimental mean diameter)
SMPS1	6-Jet collison nebulizer	Model 3071A (TSI) Long DMA—Bipolar, Kr-85	–	Water CPC, model 3787 (TSI)	Scanning; Up scan: 180 s, Down scan: 30 s, Idling time: 30 s	9	0.6	AIM software with charge corrections	CRM 3050A (46 ± 2 nm)	Scanning; <6 % for CRM 3050A
SMPS2	Atomizer model 3076 (TSI)	Model 3081 (TSI) Long DMA—Bipolar, Kr-85	0.457 mm (TSI)	UCPC, model 3025A (TSI)	Scanning; Up scan: 180 s, Down scan: 30 s, Idling time: 30 s	3	0.3	AIM software with charge and diffusion corrections Gaussian law	ISO 15900 (leak test, zero test, and flowrate calibration) CRM 3050A # 39449 (46 ± 2 nm) and CRM 3080A # 39259 (81 ± 3 nm)	Scanning; <2 % for CRM 3050A and CRM 3080A
SMPS3	Atomizer model 3076 (TSI)	Model 3081 Long DMA(TSI)—Bipolar, Kr-85	0.0457 cm (TSI)	Butanol CPC, model 3776 (TSI)	Scanning; Up scan: 180 s, Down scan: 30 s, Idling time: 30 s	3	0.3	AIM software without charge and diffusion corrections	ISO 15900 (Voltage, flow rate calibration and leak test) CRM JSR SC-010-S (100.82 ± 0.66 nm)	Scanning; <1 % for CRM
SMPS4	Atomizer model 3076 (TSI)	Model 3081 (TSI) Long DMA—Bipolar, Kr-85	0.0457 cm (TSI)	Butanol CPC, model 3022 (TSI)	Scanning; Up scan: 180 s, Down scan: 30 s, Idling time: 30 s; Stepping; For each voltage, Idling: 20 s, Counting: 10 s	3	0.3	AIM software with charge and diffusion corrections DMA moment method	ISO 15900 (Voltage, flow rate calibration and leak test) CRM 3050A (46 ± 2 nm) and CRM 3080A (83 ± 3 nm)	Scanning; <9 % for CRM 3050A and <1 % for CRM 3080A; Stepping; <2 % for CRM 3050A and CRM 3080A
SMPS5	Atomizer; (JSR) Aeromaster V; Electrospray model 3480 (TSI)	Model 3081 Long DMA (TSI)—Bipolar, Am-241	0.071 cm (TSI)	Butanol CPC, model 3022A (TSI)	Scanning; Up scan: 180 s, Down scan: 30 s, Idling time: 30 s; Stepping; For each voltage, Idling: 20 s, Counting: 10 s	19.5; 3	1.0; 0.3	AIM software with/without charge corrections DMA moment method with relative size measurement	ISO 15900 (Voltage, flow rate calibration, and leak test) CRM JSR SC-010-S (100.82 ± 0.66 nm)	Scanning; <1 % for CRM; Stepping; <1 % for CRM

Table 4 Summary of the involved atomic force microscopes

Lab	Instrument manufacturer and type	Height signal	Expanded uncertainty for 40 nm step height calibration (nm)	Image analysis software	Particle detection	Particle height evaluation	AFM tip radius (nm)
AFM1	Bruker (Veeco) Nanoman Vs	Optical sensor of the hybrid AFM head	0.7	Mountains Map from Digital Surf + own dedicated Matlab routine	Threshold + manual choice	z-maximum on the particle minus averaged surface height	<10
AFM2	Bruker DIM3100 m	Capacitive sensor	0.7	SPIP 6.0.2	User defined height threshold	z-maximum of particle above the level of mica substrate surface	<10
AFM3	Asylum Research MFP-3D SA	LVDT z-axis sensor in MFP-3D	1.0	SPIP 5.1.3	Height threshold	z-maximum of particle above the level of mica substrate surface	<10
AFM4	JEOL JSPM 5200	Feedback voltage	3.6	Image analysis software WinSPM JEOL SystemTM	Manual choice	z-maximum of particle above the level of mica substrate surface	<15

Table 5 SEM operating parameters used by each laboratory at the interlaboratory comparison

Lab	SEM instrument, product name, actual resolution	Electron source type (W, LaB6, FEG, Schottky)	Coating used	High voltage, working distance	Nominal magnification (Mag), field of view (FOV), pixel matrix, corresponding approximate number of NPs in an image	Electron detector type	Image Analysis Software (Manual or automatic delimitation of nanoparticles)	Calibration traceability of image magnification	Associated uncertainty of magnification calibration ($\pm$nm)	Other relevant remarks
SEM1	Jeol 6301F® 1.5 nm @ 30 kV 5 nm @ 1 kV	FEG	Coating: Pt Correction: yes (2.5 nm × 2)	HV = 15 kV WD = 8 mm	Mag: ×100,000 FOV: 1.2 × 0.9 μm^2 Matrix: 512 × 400 pixels NPs/image: ~10 (K50)	ET	Software: SAISAM (Microvision Instruments®) NP delimitation: manual	CRM 3080A CRM 8013	9	

Table 5 continued

Lab	SEM instrument, product name, actual resolution	Electron source type (W, LaB6, FEG, Schottky)	Coating used	High voltage, working distance	Nominal magnification (Mag), field of view (FOV), pixel matrix, corresponding approximate number of NPs in an image	Electron detector type	Image Analysis Software (Manual or automatic delimitation of nanoparticles)	Calibration traceability of image magnification	Associated uncertainty of magnification calibration ($\pm$nm)	Other relevant remarks
SEM2	Jeol 7001F 1.2 nm @ 30 kV 3.0 nm @ 1 kV	Schottky FEG	Coating: Au Correction: yes (13 nm × 2)	HV = 10 kV WD = 8 mm	Mag: ×80,000 FOV: ~ 1.5 × 1.1 μm^2 Matrix: 1,280 × 960 pixels NPs/image: ~ 20 (Aerosol DP)	ET	Software: ImageJ NP delimitation: semi-automatic or manual	CRM 8013	5	The coeff. of variation (CV) for the calibration was quite high (9.3 %), higher than would be expected from the CRM 8013
SEM3	Extra High Resolution FEI Magellan 400L 0.8 nm @ 15 kV in SE mode 0.9 nm @ 1 kV in SE mode 1.5 nm @ 200 V in SE mode 0.5 nm @ 30 kV in STEM mode	Schottky FEG, with UNICAP (monocromator)	Coating: no	HV = 1 kV WD = 2 mm	Mag: ×60,000 to ×300,000 FOV: 746 × 644 nm^2 Matrix: 1,024 × 884 pixels NPs/image: ~ 30 (Aerosol OP, ×200,000) FOV: 1,429 × 1,288 nm^2 NPs/image: ~ 50 (Aerosol DP, ×100,000)	SE with TLD in SE or charge neutralizing (CN) mode	Software: ImageJ NP delimitation: manual	Au grating SIRA Sample Calibration samples were used (AGAR S170 samples with gratings 19.7 and 2,160 lines/mm)	3	Images were acquired by integrating of 16–32 frames at 100 ns dwell time
SEM4	Jeol EPMA-JXA 8200 Theoretical resolution = 4 nm, practical resolution = around 40 nm	W	Coating: Au Correction: no, but uncertainty budget accordingly expanded	HV = 30 kV WD = 8–10 mm	Mag: ×80,000 FOV: 1.45 × 1.36 μm^2 Matrix: 480 × 386 pixels NPs/image: 15–40	ET	Software: Scion Image Corporation, NP delimitation: manual	CRM 8013, CRM NIST SRM-1963 (PSL of 100.7 $\pm$ 1.0 nm)	10	

Table 5 continued

Lab	SEM instrument, product name, actual resolution	Electron source type (W, LaB6, FEG, Schottky)	Coating used	High voltage, working distance	Nominal magnification (Mag), field of view (FOV), pixel matrix, corresponding approximate number of NPs in an image	Electron detector type	Image Analysis Software (Manual or automatic delimitation of nanoparticles)	Calibration traceability of image magnification	Associated uncertainty of magnification calibration (±nm)	Other relevant remarks
SEM5	Zeiss Gemini LEO 1525 FE-SEM, 1.5 nm @ 20 kV, 3.5 nm @ 1 kV	FEG	Coating: Au/Pd, Correction: no, but uncertainty budget correspondingly expanded	HV = 8 kV, WD = 2 mm	Mag: ×100,000, FOV: 3.7 × 2.6 μm², Matrix: 1,036 × 829 pixels, NPs/image: ~100, Mag: ×200,000, FOV: 1.9 × 1.3 μm², Matrix: 1,036 × 829 pixels, NPs/image: ~20	Inlens	Software: ImageJ, NP delimitation: automated, after thresholding manual elimination of obvious artefacts	CRM 8012 and CRM 8013 were used for comparison with NIST SRM 484 g	7	
SEM6	Zeiss Supra 40, 3.5 nm @ 20 kV, 6 nm @ 1 kV[a]	Schottky (thermally assisted) field emitter	Coating: Au of different thickness, also no coating, Correction: yes (manually by checking the same coating conditions on Si substrates)	HV = 5–30 kV, WD = 5 mm	Mag: ×50,000, FOV: ~5 × 5 μm², Matrix: 1,024 × 768 pixels, NPs/image: ~200, Mag: ×250,000, FOV: ~1 × 1 μm², Matrix: 1,024 × 768 pixels, NPs/image: ~20	InLens and ET	Software: ImageJ, NP delimitation: automated, however, after eliminating manually the overlapping NPs or other noticeable artefacts	CD calibration structure 10-5-2-1-0.5 mm (with PTB certificate)	5	
SEM7	Zeiss Supra 40 VP, 1.0 nm @ 15 kV, 1.9 nm @ 1 kV	W	Coating: no	HV = 20 kV, WD = 8.5 mm	Mag: ×100,000 to ×500,000, FOV: ~1 × 0.7 μm², Matrix: 1,024 × 768 pixels, NPs/image: ~20 (Aerosol OP, ×200,000)	SE and InLens	Software: ImageJ, NP delimitation: manual	CRM 3030A, CRM 3080A, CRM 8012, CRM 8013	4	

[a] Resolution figure determined with SMART software (© David Joy, University of Tennessee, USA)

Table 6 TEM operating parameters used by each laboratory during the interlaboratory comparison

Lab	TEM manufacturer name	Electron source type (W-fil, LaB6 or FEG)	Accelerating voltage (kV)/ magnification	Microscope mode for imaging (TEM or STEM)	Imaging mode: Bright Field TEM with or without objective aperture, size of aperture if used) STEM mode: Bright Field, Dark Field of High angular annular DF	Recording device (plates of CCD camera)	CCD camera name and type CCD, size (1, 2K, 4K or 6K), binning and integration time	Image Analysis Software (Manual or automatic delimitation of nanoparticles)	Traceability
TEM1	FEI Tecnai F30 STWIN 0.2 nm UTWIN 0.17 nm	FEG	300 kV/×39,000 (nominal magnification)	TEM	BF TEM with OA (size of OA = 70 μm)	CCD camera (2k × 2k)	UltraScan (Gatan, Inc), 2k × 2k, without binning, 1 s	ImageJ (Manual delimitation of nanoparticles)	(Lattice constant of silicon)
TEM2	TEM Jeol 100 CXII with detector PGT®/Si(Li) Resolution 0.3 nm	W	100 kV/magnification used ×190,000 and ×270,000	TEM	Bright field	CCD Camera	CCD camera (300 W Dualvision GATAN® model 780) Image Size: 2621 K (1,300 × 1,030 pixels) Binning:1 integration time:auto exposure	Software package SAISAM from Microvision Instruments® (Manual delimitation of nanoparticles)	Calibrated using the supplied standard PLS and gold particles CRM 3080A (81.0 ± 3.0 nm) CRM 8012 (27.6 ± 2.1 nm)
TEM3	JEOL-2100 TEM Resolution 0.23 nm	LaB6	200 kV, usual magnification = ×30,000 (some images were taken at ×40K and ×50K)	TEM	Bright field TEM with objective aperture #2 (50 μm)	CCD camera	Gatan Orius bottom-mount CCD camera (4K × 2K), image size 4,008 × 2,672 pixels, no binning, integration time 2 s	ImageJ (semi-automatic delimitation of nano-particles, manual where necessary)	Calibrated using the supplied standard PSL and gold nanoparticle samples
TEM4	HR FEG TEM Tecnai F20 G2 (FEI Company) STWIN 0.24 nm	Schottky –type FEG	200 kV 10K–40K on a screen	TEM mode	Bright field imaging	CCD 1K × 1K GATAN MS 794	GATAN SSCCD camera MSC794 of 1k × 1k size at integration time of 0.4 s without binning 1,024 × 1,024 pixels full field of view	ImageJ, automatic delimitation of nanoparticles	Calibrated on Gold cross-grating sample AGAR S106/S107 2160 lines/mm

Table 6 continued

Lab	TEM manufacturer name	Electron source type (W-fil, LaB6 or FEG)	Accelerating voltage (kV)/magnification	Microscope mode for imaging (TEM or STEM)	Imaging mode: Bright Field TEM with or without objective aperture, size of aperture if used) STEM mode: Bright Field, Dark Field of High angular annular DF	Recording device (plates of CCD camera)	CCD camera name and type CCD, size (1, 2K, 4K or 6K), binning and integration time	Image Analysis Software (Manual or automatic delimitation of nanoparticles)	Traceability
TEM5	TEM Jeol 2100 Resolution 0.23 nm	LaB6	100 kV, magnification used around ×30K	TEM	Bright field with objective aperture #3 (40 μm)	CCD camera	Gatan Ultrascan 1,000 (2K × 2K), binning: 1, integration time: 1 s	Image J, automatic delimitation of the particles	Calibrated using the supplied PSL 80 nm particles
TEM6	TEM JEOL JEM 2010 Resolution 0.23 nm	LaB6	200 kV/mag 50K–250K	TEM	Bright field imaging			Image J (manual delimitation of nanoparticles)	Calibrated using the supplied standard PSL and gold nanoparticle samples
TEM7	Zeiss Supra 40, working in the transmission mode, i.e. T-SEM	Schottky-FEG	10–30 kV	T-SEM option	Bright-field T-SEM (using a special setup which trapped the SE/BSE on their "direct" way to the conventional ET detector and with an Au convertor under the thin sample for multiplication of the transmitted (only) electrons which are then collected by the ET detector)	–	Software: ImageJ NP delimitation: automated, however, after eliminating manually the stuck NPs or other noticeable artefacts	CD calibration structure 10-5-2-1-0.5 mm (with PTB certificate) measured in the conventional SEM mode and extended to the T-SEM mode Also counter-checked with CRM 3030A, CRM 3080A, CRM 8012, CRM 8013

Table 7 SMPS measurement results of mean and mode diameters of aerosol OP

Lab	Operating mode	Mean				Mode				SD (nm) or GSD	Used range (nm)
		d_m (nm)	σ_R (nm)	u (nm)	U (nm)	d_m (nm)	σ_R (nm)	u (nm)	U (nm)		
SMPS1	Scanning 1	34.7	0.6	1.9	3.9	34.7	0.7	0.7	1.3	1.1	28.4–42.2
SMPS2	Scanning 1	36.0*	1.1*	1.1	2.2	36.0	1.1	1.1	2.2	5.9 nm*	–
	Scanning 2	34.0	0.1	1.8	3.7					1.2	25.0–42.9
SMPS3	Scanning 1	42.6	0.6	1.9	3.9	37.2	0.5	0.5	1.0	1.3	14.6–430
SMPS4	Scanning 1	32.2	0.8	2.0	4.0	34.7	0.4	0.4	0.8	1.4	14–434
	Scanning 2	34.2	0.2	1.8	3.7					1.1	25.0–42.9
SMPS5	Scanning 1	33.4	0.2	1.8	3.7	34.6	0.2	0.3	0.5	1.2	14.1–710.5
	Stepping	34.0	0.1	0.4	0.8	35.6	0.0	0.4	0.8	3.1 nm**	21.2–45.1

σ_R (standard deviation of reproducibility), u (combined standard measurement uncertainty), U (expanded uncertainty with the coverage factor $k = 2$). OP ("*" values were determined with a Gaussian law of the AIM results, "**" values were determined with a Asymmetric Gaussian law, "GSD" values were determined by a log-normale law, r = repeatability and R = Reproducibility)

Table 8 SMPS measurement results of mean and mode diameters of aerosol DP

Lab	Operating mode	First population									
		Mean				Mode				SD (nm) or GSD	Used range (nm)
		d_m (nm)	σ_R (nm)	u (nm)	U (nm)	d_m (nm)	σ_R (nm)	u (nm)	U (nm)		
SMPS1	Scanning 1	45.2	1.7	6.7	13.3	46.0	0.5	9.5	18.9	1.1	40.7–52.3
SMPS2	Scanning 1	45.3*	0.9*	9.5	19.0	45.3	0.9	9.5	19.0	6.5 nm*	–
	Scanning 2	45.2	0.2	6.4	12.9					1.1	37.2–55.2
SMPS3	Scanning 1	45.0	0.5	6.5	12.9	39.0	5.7	11.0	22.1	1.1	37–55.2
SMPS4	Scanning 1	44.4	0.1	6.4	12.9	44.7	0.5	9.5	18.9	1.1	37.2–55.2
	Scanning 2										
SMPS5	Scanning 1	39.9	0.2	6.4	12.9	44.4	0.4	9.5	18.9	1.3	14.1–51.4
	Stepping	42.7	0.1	1.2	2.5	46.1	0.1	0.8	1.5	7.4 nm**	29.7–99.3

Table 8 continued

Lab	Operating mode	Second population									SD (nm) or GSD	Used range (nm)	Peak ratio (%)	Area ratio (%)
		Mean				Mode								
		d_m (nm)	σ_R (nm)	u (nm)	U (nm)	d_m (nm)	σ_R (nm)	u (nm)	U (nm)					
SMPS1	Scanning 1	82.2	0.5	2.2	4.3	82.2	0.6	2.2	4.3	1.1	67.3–100	52	63
SMPS2	Scanning 1	85.1*	0.0*	2.1	4.2	85.1	0.0	2.1	4.2	7.0 nm*	–	21	18
	Scanning 2	85.6	0.3	2.1	4.3					1.1	61.5–101.8	21	26
SMPS3	Scanning 1	87.9	0.5	2.2	4.3	81.9	0.5	2.2	4.3	1.2	61.5–661.2	40	–
SMPS4	Scanning 1	87.6	0.4	2.1	4.3	82.1	0.0	2.1	4.2	1.2	63.8–429.4	20	29
	Scanning 2	83.0	0.1	2.1	4.2					1.1	61.5–101.8	20	33
SMPS5	Scanning 1	84.8	0.2	2.1	4.2	82.1	0.0	2.1	4.2	1.1	53.3–710.5	19	36
	Stepping	83.5	0.0	0.7	1.5	85.5	0.0	0.8	1.6	3.9 nm**	29.7–99.3	16	29

σ_R (standard deviation of reproducibility), u (combined standard measurement uncertainty), U (expanded uncertainty with the coverage factor $k = 2$)/("*" values were determined with a Gaussian law of the AIM results, "**" values were determined with an asymmetric Gaussian law, "GSD" values were determined by a log-normal law, r = repeatability and R = reproducibility, peak ratio were calculated as = minor peak intensity/major peak intensity (in %), Area ratio as = ratio in number concentration between the first and the second populations (in %)

Table 9 AFM measurement results for aerosol OP (the same sample on a mica substrate, indicated by "M*", performed by laboratory SMPS4, was measured by laboratories AFM1, 2, and 4)

Sampling lab	Samples	Support name (grids:G, N or Mica; M or filter; H)	AFM Lab	Mode Diameter d_h (nm)	Mode Uncertainty (±nm) (2k)	Mode Average (nm)	Mode 2*SD, reproducibility (nm)	Mean Diameter d_h (nm)	Mean Uncertainty (±nm) (2k)	Mean Average (nm)	Mean 2*SD, reproducibility (nm)	Distribution SD size distribution (nm) (gaussian law)	Distribution Range (nm)
SMPS4	A	G2		31.9	6.3	31.0	2.7	29.2	6.2	29.7	1.4	5	full range
		G2	AFM1	30.0	4.9			30.2	4.8			4.3	full range
	B	N3		32.7	2.4	31.9	2.4	30.9	2.2	30.6	0.5	3.2	full range
		N3	AFM1	30.5	2.0			30.4	1.8			3.4	full range
		N4		32.5	2.2			30.5	1.8			3.5	full range
	D	M*		32.0	2.2	-	-	30.9	1.7	-	-	3.3	full range
		M*	AFM2	31.7	3.3			30.5	1.6			8.6	full range
		M*	AFM4	29.0				34.9	3.6			12.1	8.2 - 84.7
SMPS2	A	G1	AFM2	27.4	3.1	25.4	5.8	26.8	2.3	28.3	4.1	7	15 - 60
		G2	AFM2	23.3	2.8			29.7	2.9			6.4	15 - 60
		G2	AFM1	30.3	5.4	-	-	29.2	5.2	-	-	3.8	full range
SMPS3	D	M	AFM3	28.0		-	-	28.0	0.9	-	*	4.5	10 - 45
		M		31.4	3.3	32.0	1.1	30.2	7.3	31.2	2.4	6.1	10 - 60
		M	AFM2	32.5	3.0			32.5	2.3			5.2	10 - 60
		M		32.1	3.4			30.9	3.9			4.7	10 - 60

Table 10 AFM measurement results of aerosol DP (the same sample on a mica substrate, indicated by "M*", performed by laboratory SMPS4, was measured by laboratories AFM1 and 2)

Sampling lab	Samples	Support name (grids:G, N or Mica; M or filter; H)	AFM lab	1st population — Mode Diameter d_h (nm)	1st population — Mode Uncertainty (±nm) (2k)	1st population — Mean Diameter d_h (nm)	1st population — Mean Uncertainty (±nm) (2k)	1st population — SD size distribution (nm) (gaussian law)	1st population — Range (nm)	2nd population — Mode Diameter d_h (nm)	2nd population — Mode Uncertainty (±nm) (2k)	2nd population — Mean Diameter d_h (nm)	2nd population — Mean Uncertainty (±nm) (2k)	2nd population — SD size distribution (nm) (gaussian law)	2nd population — Range (nm)	1st/2nd Peak ratio (%)	1st/2nd Area ratio (%)
SMPS4	A	G2	AFM1	39.0	5.2	36.2	5.1	6.6	full range	80.0	5.2	77.9	5.1	5.1	full range	81.4	-
SMPS4	B	N3	AFM1	40.6	2.7	39.8	2.0	6	full range	83.7	2.7	82.2	2.0	4.5	full range	74.3	-
SMPS4	D	M*	AFM1	44.6	2.5	41.7	2.2	7.8	full range	86	2.5	84.5	2.2	4.3	full range	24.9	-
SMPS4	D	M*	AFM2	35.9	2.0	34.7	1.5	8.8	0 - 60	79.9	2.7	79.1	1.9	6.7	60 - 100	158.0	192.5
SMPS2	A	G2	AFM1	35.9	3.5	35.7	2.6	5.8	full range	78.2	3.5	77.7	2.6	5.0	full range	57.7	-
SMPS2	A	G1	AFM2	36.1	2.4	34.1	3.2	7.6	0 - 60	78.1	3.1	77.9	3.4	6.1	60 - 100	45.8	70.4
SMPS3			AFM3	42.0	-	41.4	2.0	8.8	17 - 54	84.0		83.6	1.9	8.7	56 - 100	34.3	-
SMPS3	D	M	AFM2	-	-	33.2	4.2	9.2	0 - 60	80.1	3.2	80.2	4.3	5.7	60 - 100	-	50.0
SMPS3	D	M	AFM2	-	-	31.8	2.3	9.8	0 - 60	80.7	3.3	80.4	2.6	6.5	60 - 100	-	68.8
SMPS3	D	M	AFM2	-	-	33.6	2.5	9.4	0 - 60	79.5	2.5	78.2	2.7	5.9	60 - 100	-	78.1

Table 11 SEM measurement results for aerosol OP

SEM	Sampling lab	Samples	SEM lab	Mode Diameter d_p (nm)	Mode Uncertainty (±nm) (2k)	Mode Average (nm)	Mode 2*SD, reproducibility (nm)	Mean Diameter d_p (nm)	Mean Uncertainty (±nm) (2k)	Mean Average (nm)	Mean 2*SD, reproducibility (nm)	SD of the size distribution	Range (nm); *: with coating	Remarks
SEM	SMPS4	C	SEM6	32	15.0	32.7	8.1	34.6	15.0	36.1	2.8	7.2	32 – 77 *	Au coating, correction (20 nm)
				29	15.0			36.1	15.0			7.6	28 – 87 *	
				37	15.0			37.4	15.0			8.5	30 – 93 *	
			SEM7	35.5	5.0	35.8	1.2	35.7	5.0	36.2	1.7	4.0	23–47	Without coating
				35.5	5.0			35.8	5.0			5.4	22–58	
				36.5	5.0			37.2	5.0			6.8	24–71	
			SEM3	36	4.0	36.7	1.2	35.4	4.0	35.8	1.4	4.1	22 – 50	Without coating
				37	4.0			36.6	4.0			4.6	21 – 85	
				37	4.0			35.3	4.0			4.4	18 – 53	
			SEM5	43.7	32.0	40.8	13.6	49.0	32.0	48.9	2.4	10.2	32 – 105 *	Au/Pd coating; not corrected for coating thickness, but included into uncertainty
				33.1	32.0			47.6	32.0			10.7	32 – 77 *	
				45.7	32.0			50.0	32.0			10.6	32 – 83*	
	SMPS2		SEM4	53.8	10.0	53.1	4.1	51.3	10.0	50.6	1.6	6.0	33 – 64*	Au coating; not corrected for coating thickness, but included into uncertainty, Traceable to NIST SRM 8013
				54.7	10.0			50.8	10.0			4.8	24 – 63*	
				50.8	10.0			49.7	10.0			2.7	32 – 63*	
				42.5	10.0	41.9	3.2	40.6	10.0	40.0	1.3	4.8	26 – 51*	Au coating; not corrected for coating thickness, but included into uncertainty, Traceable to NIST SRM 1963
				43.2	10.0			40.2	10.0			3.8	19 – 49*	
				40.1	10.0			39.3	10.0			4.6	26 – 50	
	SMPS3		SEM3	32	4.0	31.3	2.3	31.2	4.0	30.8	0.9	3.0	22 – 44	Without coating
				32	4.0			30.9	4.0			3.3	18 – 40	
				30	4.0			30.4	4.0			3.8	18 – 45	
			SEM7	33.5	5.0	33.8	1.2	33.7	5.0	33.9	0.6	4.0	23–74	Without coating
				33.5	5.0			33.7	5.0			5.9	19–67	
				34.5	5.0			34.2	5.0			6.8	17–82	

Table 12 SEM measurement results of aerosol DP

Sampling lab	Samples	SEM lab	1st Mode d_p (nm)	1st Mode Uncert (±2k) (nm)	1st Mode Average (nm)	1st Mode 2*SD repro (nm)	1st Mean d_p (nm)	1st Mean Uncert (2k) (±nm)	1st Mean Average (nm)	1st Mean 2*SD repro (nm)	1st Dist SD (nm)	1st Dist Range (nm); * with coating	2nd Mode d_p (nm)	2nd Mode Uncert (2k) (±nm)	2nd Mode Average (nm)	2nd Mode 2*SD repro (nm)	2nd Mean d_p (nm)	2nd Mean Uncert (2k) (±nm)	2nd Mean Average (nm)	2nd Mean 2*SD repro (nm)	2nd Dist SD	2nd Dist Range (nm); *: with coating	Peak ratio (%)	Area ratio (%)	Remarks
SMPS4	c	SEM6	46	15.0	48.3	6.4	46.1	15.0	47.8	4.7	12.2	22 – 90 (*)	93	20.0	96.0	5.3	95.7	20.0	97.5	4.9	8.1	91 – 200 (*)	31	32	With Au coating, correction (20 nm)
			52	15.0			46.7	15.0			12.0	7 – 90 (*)	97	20.0			96.4	20.0			8.8	91 – 200 (*)	32	23	
			47	15.0			50.5	15.0			10.1	10 – 90 (*)	98	20.0			100.3	20.0			9.4	91 – 200 (*)	33	22	
		SEM7	43	5.0	43.3	5.0	43.4	5.0	44.5	2.0	6.8	24-60	85	5.0	85.3	3.1	84.1	5.0	89.6	1.0	6.1	63-103	25	26	Without coating
			46	5.0			44.8	5.0			6.1	27-63	84	5.0			84.5	5.0			5.2	67-98	38	30	
			41	5.0			45.3	5.0			6.4	29-64	87	5.0			85.1	5.0			6.0	66-102	28	21	
		SEM3	43	4.0	44.3	3.1	45.1	4.0	45.1	1.2	5.9	28-61	83	4.0	83.7	1.2	82.5	4.0	82.5	0.8	5.3	63-97	34	34	Without coating
			46	4.0			44.6	4.0			5.9	25-58	84	4.0			82.1	4.0			5.3	61-101	42	42	
			44	4.0			45.8	4.0			6.5	26-61	84	4.0			82.8	4.0			4.9	66-98	24	24	
		SEM1	57.6	10.0	57.8	1.6	57.9	10.0	57.6	1.5	6.6	39 – 83 (*)	99.9	10.0	100.9	2.6	99.6	10.0	100.3	2.0	5.8	84 – 127 (*)	19	23	With Pt coating, correction (5nm)
			58.7	10.0			58.2	10.0			6.5	45 – 78 (*)	102.4	10.0			101.5	10.0			5.8	80 – 125 (*)	17	23	
			57.1	10.0			56.8	10.0			7.0	38 – 80 (*)	100.5	10.0			99.9	10.0			5.7	81 – 119 (*)	23	26	
		SEM5	37.5	32.0	48.6	19.3	48.9	32.0	50.4	3.9	10.2	33-70 (*)	89.6	32.0	96.1	12.1	92.1	32.0	96.1	7.0	8.7	70-114 (*)	50	37	With Au/Pd coating; not corrected for coating thickness, but included in uncertainty
			53.0	32.0			52.6	32.0			10.9	35-75 (*)	97.1	32.0			98.6	32.0			6.4	79-108 (*)	42	55	
			55.2	32.0			49.6	32.0			10.6	32-77 (*)	101.6	32.0			97.5	32.0			6.5	78-107 (*)	33	53	
SMPS2			50.4	10.0	52.2	3.2	51.5	10.0	51.6	0.4	6.4	37 – 63 (*)	107.6	10.0	107.5	1.3	102.7	10.0	101.9	1.4	8.3	80 – 117 (*)	51	47	Au coating; not corrected for coating thickness, but included into uncertainty, Traceable to NIST SRM 8013
			53.4	10.0			51.8	10.0			5.7	32 – 61 (*)	106.9	10.0			101.4	10.0			6.3	75 – 116 (*)	36	40	
			52.8	10.0			51.4	10.0			5.7	31 – 60 (*)	108.2	10.0			101.7	10.0			6.5	83 – 117 (*)	62	59	
		SEM4	43.0	10.0	42.3	1.2	40.7	10.0	40.7	0.3	5.6	29 – 50 (*)	85.1	10.0	85.0	1.0	81.2	10.0	80.6	1.1	6.6	62 – 93 (*)	51	47	Au coating; not corrected for coating thickness, but included into uncertainty, Traceable to NIST SRM 1963
			42.3	10.0			40.9	10.0			4.5	25 – 48 (*)	84.5	10.0			80.2	10.0			5.0	62 – 92 (*)	36	43	
			41.8	10.0			40.6	10.0			4.8	25 – 48 (*)	85.5	10.0			80.4	10.0			5.2	65 – 92 (*)	62	59	
		SEM1	58.2	10.0	58.2	0.4	57.9	10.0	57.8	0.5	6.9	41 – 76 (*)	103.6	10.0	102.9	4.4	102.9	10.0	102.4	4.5	6.9	80 – 130 (*)	27	20	With Pt coating, correction (5nm)
			58.4	10.0			58.0	10.0			6.5	36 – 80 (*)	104.6	10.0			104.4	10.0			6.8	82 – 159 (*)	19	20	
			58.0	10.0			57.5	10.0			7.0	43 – 80 (*)	100.4	10.0			100.0	10.0			5.7	80 – 124 (*)	15	23	
SMPS3		SEM2	41	15.0	36.0	14.1	37.5	15.0	32.3	14.5	5.6	51 – 73 (*)	89	15.0	80.0	25.5	82.8	15.0	74.0	24.9	11.7	84 – 196 (*)	24	10	With Au coating, correction (26 nm)
			31	15.0			27.2	15.0			4.7	43 – 61 (*)	71	15.0			65.2	15.0			9.8	70 – 164 (*)	26	10	
		SEM3	42	4.0	41.0	2.0	41.3	4.0	41.4	1.8	6.3	17 – 55	81	4.0	81.0	2.0	78.6	4.0	80.0	2.7	6.1	55 – 93	42	42	Without coating
			40	4.0			40.5	4.0			5.8	24 – 52	80	4.0			80.1	4.0			5.4	57 – 97	41	41	
			41	4.0			42.3	4.0			5.6	27 – 57	82	4.0			81.2	4.0			5.7	65-100	33	33	
		SEM7	44.5	5.0	45.2	1.5	42.3	5.0	43.8	3.6	6.6	21-64	82	5.0	82.7	1.2	81.8	5.0	83.2	2.4	5.7	65-100	27	27	Without coating
			46	5.0			43.4	5.0			5.5	24-65	83	5.0			83.6	5.0			5.0	66-105	20	19	
			45	5.0			45.8	5.0			5.5	31-64	83	5.0			84.1	5.0			5.4	67-102	36	36	

a With coating

Table 13 Size measurements of silica Aerosol OP by TEM

Sampling lab	Samples	Name of the grids (N1, N2,... G1,... or g1...)	TEM Lab	Mean			Mode			SD of size distribution (nm)
				Diameter d_p (nm)	Average (nm)	2*SD, reproducibility (nm)	Diameter d_g (nm)	Average (nm)	2*SD, reproducibility (nm)	
SMPS3	A	G1	TEM4	29.5	28.9	1.6	31.0	30.5	1.2	6.6
		G1		29.3			30.0			4.7
		G1		27.8			31.0			6.3
		G1		29.2			30.0			4.5
	B	G1	TEM3	32.3	-	-	34.0	-	-	3.0
		N1	TEM1	35.3	-	-	31.3	-	-	2.9
		N3	TEM5	35.9	-	-	37.3	-	-	3.7
	A	G2		28.8			30.0			4.2
		G2	TEM4	28.3	28.7	0.8	31.0	30.3	1.2	6.0
		G2		29.1			30.0			5.1
		N3		28.7			29.0			4.0
	B	G1	TEM1	35.8	36.0	0.5	-	-	-	3.9
		G1		36.2			31.1			3.6
		N1		35.0						3.5
SMPS4	A	G1*		36.5			37.1			4.4
		G1		37.1	36.8	0.6	37.4	37.3	0.3	4.6
		G1		36.9			37.4			4.4
		g1	TEM2	52.9			52.9			4.2
		g1		54.0	53.6	1.2	54.4	53.6	1.5	4.1
		g1		53.8			53.6			4.2
	B	N1		36.4			36.8			4.2
		N2		37.7	36.8	1.6	38.3	37.3	1.8	4.5
		N3		36.2			36.7			4.4
	A	G1		39.5			40.0			7.2
		G2		37.4			33.0			7.1
		G2		40.9			43.0			6.0
		G2	TEM7	39.3	39.2	1.9	39.0	39.8	6.8	5.5
		G1		39.0			39.0			5.1
		G1		39.3			43.0			5.1
		G2*		39.1			43.0			6.0
	B	N1		39.0	-	-	38.0	-	-	6.0
				40.0			40.0			5.0
SMPS2	B	G1	TEM5	35.9	35.8	0.2	35.5	36.4	2.5	5.1
		G2		35.7			37.3			4.0
		G1		37.9			33.0			15.0
		G2		37.3			37.0			6.3
	A	G1	TEM3	35.0	34.9	4.9	37.0	35.3	3.0	7.4
		G1		33.1			35.0			3.0
		G2		31.4			35.0			3.2
		G2		34.9			35.0			7.8
		G1		36.6			37.0			4.1
		G1	TEM2	36.8	37.1	1.5	37.2	37.5	1.4	3.8
		G1		38			38.3			3.9
		g1		51.7	52.3	1.3	52.2	52.6	1.1	4.1
		g1		53			53.2			4.2
		g1		52.1			52.4			4.1
SMPS1	A	G1	TEM3	32.2	32.8	1.9	35.0	35.0	0.0	2.7
		G2		33.5			35.0			3.5
	C	g1		30.7	-	-	31.0	-	-	3.1

* Indicates that this sample measured is the same TEM Grid sample performed by laboratory SMPS4

Table 14 Size measurements of silica Aerosol DP by TEM

	Sampling lab	Samples	Name of the grids (N1, N2, GI…, gI…)	TEM Lab	1st population Mean Diameter dp (nm)	1st pop Mean Average (nm)	1st pop Mean 2*SD reproducibility (nm)	1st pop Mode Diameter dp (nm)	1st pop Mode Average (nm)	1st pop Mode 2*SD reproducibility (nm)	1st pop SD of size distribution (nm)	2nd population Mean Diameter dp (nm)	2nd pop Mean Average (nm)	2nd pop Mean 2*SD reproducibility y (nm)	2nd pop Mode Diameter dp (nm)	2nd pop Mode Average (nm)	2nd pop Mode 2*SD reproducibility (nm)	2nd pop SD of size distribution (nm)
TEM	SMPS3	A	G1	TEM4	35.0	34.6	2.2	29.0	31.0	3.5	4.8	77.6	77.8	3.2	80.0	80.0	4.0	5.30
			G1		33.3			32.0			4.7	76.3			78.0			6.13
			G1		35.4			32.0			4.7	79.4			82.0			5.92
			G1	TEM3	39.9			45.0			5.3	79.9			85.0			5.36
			N1	TEM1	43.2						5.7	82.2						4.06
		B	N3	TEM5	44.3			44.4			5.8	87.5			90.6	90.6		5.45
	SMPS4	A	G2	TEM4	36.0	35.2	1.4	38.0	36.0	5.3	6.4	80.1	79.5	1.5	81.0	81.0	2.0	6.06
			G2		34.8			33.0			5.4	79.7			82.0			5.90
			N4		34.8			37.0			5.6	78.7			80.0			6.23
			G1		34.5			38.0			4.9	76.6			78.0			6.28
			N1	TEM1	43.6	43.9	0.9				5.4	81.2	82.6	4.2				5.57
			G1*		44.2						6.3	84.1						4.26
			G1		41.2						5.9	82.0						5.13
			G1	TEM2	45.6	45.1	1.0	46.4*	46.0	0.4	7.0	90.3	89.9	1.6	90.9	90.6	1.5	5.2*
			g1		45.1			46.1			7.2	90.5			91.2			5.50
			g1		44.6			45.8			7.0	89.0			89.8			5.40
			N1	TEM6	63.6	63.6	0.0	64.0	64.0	0.0	6.6	109.6	109.1	1.6	110.4	109.6	2.4	6.10
			N2		63.6			64.0			7.8	108.5			108.7			5.70
			N3	TEM7	45.9	46.4	1.2	46.9	47.5	1.0	7.0	91.5	92.1	1.1	91.5	92.3	1.7	5.40
			G1		46.2			47.8			7.3	92.3			92.2			5.60
			G1		47.1			47.8			6.9	92.5			93.2			5.40
		B	G2		41.7			42.5			7.3	85.4			87.5			4.38
			G1	TEM7	48.1	46.2	2.4	49.0	48.3	4.7	9.1	93.9	93.0	3.6	92.0	94.4	4.9	5.34
			G2		45.8			50.0			8.9	91.7			96.0			6.07
			G1		46.8			49.0			9.0	93.5			96.0			5.99
			G2		46.6			49.0			8.6	94.0			95.0			7.67
			G2		44.6			43.0			8.3	89.9			90.0			5.90
			G1*		46.5			49.0			10.1	95.4			96.0			6.31
			N1		45.0			49.0			8.8	92.4			96.0			6.89
			G1		42.7			43.0			8.6	91.0			86.0			5.54
	SMPS2	A	G1	TEM5	43.5	44.0	1.5	46.2	44.4	5.0	6.3	87.5	87.8	0.8	88.8	89.7	2.5	4.80
			G2		44.6			42.6			6.1	88.1			90.6			5.20
			G1	TEM2	47.3	48.4	1.9	48.1	49.0	1.6	6.8	90.9	92.0	2.4	91.6	92.6	2.2	5.40
			G1		48.7			49.1			6.4	91.7			92.5			5.90
			G1		49.1			49.7			6.4	93.3			93.8			5.80
	SMPS1	A	G1	TEM3	42.9	42.5	0.9	43.0	43.0	0.0	5.4	78.9	79.2	0.7	81.0	80.0	2.8	5.96
			G2		42.2			43.0			3.5	79.4			79.0			3.64
		B	N4		44.2			47.0			2.3	79.0			82.0			4.14

* Indicates that this sample measured is the same TEM Grid sample performed by laboratory SMPS4

References

AFSSET (2006) Les nanomatériaux, effets sur la santé de l'homme et de l'environnement. Agence française de sécurité sanitaire de l'environnement et du travail

Allen MD, Raabe OG (1985) Slip correction measurements of spherical solid aerosol particles in an improved Millikan apparatus. Aerosol Sci Technol 4:269–286

Asbach C, Kaminski H, Fissan H, Monz C, Dahmann D, Mülhopt S, Paur HR, Heinz JK, Herrmann F, Voetz M, Kuhlbusch T (2009) Comparison of four mobility particle sizers with different time resolution for stationary exposure measurements. J Nanopart Res 11:1593–1609

Bau S, Ouf FX, Miquel S, Rastoix O, Witschger O (2010) Experimental measurement of the collection efficiency of nanoparticles samplers based on electrostatic and thermophoretic precipitation. International Aerosol Conference, August 29–September 3, 2010, Helsinki, Finlande

Buhr E, Senftleben N, Klein T, Bergmann D, Gnieser D, Frase CG, Bosse H (2009) Characterization of nanoparticles by scanning electron microscopy in transmission mode. Meas Sci Technol 20:084025

Cadle SH, Mulawa PA (1990) Atmospheric carbonaceous species measurement methods comparison study: general motors results. Aerosol Sci Technol 12:128–141

Calzolai G, Chiari M, Lucarelli F, Mazzei F, Nava S, Prati P, Valli G, Vecchi R (2008) PIXE and XRF analysis of particulate matter samples: an inter-laboratory comparison. Nucl Instrum Methods Phys Res B 266:2401–2404

Collins TJ (2007) Image J for microscopy. Biotechniques 43(1 Suppl):25–30

Countess RJ (1990) Interlaboratory analyses of carbonaceous aerosol samples. Aerosol Sci Technol 12(1):114–121

Cyrs WD, Boysen DA, Casuccio G, Lersch T, Peters TM (2010) Nanoparticle collection efficiency of capillary pore membrane filters. J Aerosol Sci 41:655–664

Dixkens J, Fissan H (1999) Development of an electrostatic precipitator for off-line particle analysis. Aerosol Sci Technol 30:438–453

EC (2009) Preparing for our future: developing a common strategy for key enabling technologies in the EU, COM

EC (2011a) Key Enabling Technologies- Final - Report June 2011

EC (2011b) Commission recommendation on the definition of nanomaterials. Brussels

Ehara K, Mulholland GW, Hagwood RC (2000) Determination of arbitrary moments of aerosol size distribution from measurements with a differential mobility analyzer. Aerosol Sci Technol 32:434–452

Environmental Protection Agency (1987) Federal register. Rules Regul 52(210):41880–41881

Fissan H, Hummes D, Stratmann F, Büscher P, Neumann S, Pui DYH, Chen D (1996) Experimental comparison of four differential mobility analyzers for nanometer aerosol measurements. Aerosol Sci Technol 24:1–13

Giechaskiel B, Dilara P, Andersson J (2008) Particle measurement programme (PMP) light-duty inter-laboratory exercise: repeatability and reproducibility of the particle number method. Aerosol Sci Technol 42:528–543

Hering SV, Appel BR, Cheng W, Salaymeh F, Cadle SH, Mulawa PA, Cahill TA, Eldred RA, Surovik M, Fitz D, Howes JE, Knapp KT, Stockburger L, Turpin BJ, Huntzicker JJ, Zhang X, McMurry PH (1990) Comparison of sampling methods for carbonaceous aerosols in ambient air. Aerosol Sci Technol 12:200–213

ISO (1994) Accuracy (trueness and precision) of measurement methods and results—part 2: basic method for the determination of repeatability and reproducibility of a standard measurement method, ISO 5725-2

ISO (2007) Workplace atmospheres—ultrafine, nanoparticle and nanostructured aerosols—inhalation exposure characterization and assessment, ISO/TR 27628

ISO (2009) Determination of particle size distribution-differential electrical mobility analysis for aerosol particles, ISO 15900

ISO (2010) Conformity assessment—general requirements for proficiency testing, ISO 17043

ISO (2011) Workplace atmosphere characterization of ultrafine aerosols/nanoaerosols—determining the size distribution and number concentration using differential electrical mobility analyzing systems, ISO 28439

ISO (2012) Air quality—sampling conventions for airborne particle deposition in the human respiratory system, ISO/CD 13138

Jeong C-H, Evans GJ (2009) Inter-comparison of a fast mobility particle sizer and a scanning mobility particle sizer incorporating an ultrafine water-based condensation particle counter. Aerosol Sci Technol 43:364–373

Lahmani M, Marano F, Houdy P (2010) Les nanosciences. Tome 4: Nanotoxicologie et nanoéthique. Paris, éditions Belin

Li C, Liu S, Zhu Y (2010) Determining ultrafine particle collection efficiency in a nanometer aerosol sampler. Aerosol Sci Technol 44:1027–1041

Maynard AD, Kuempel ED (2005) Airborne nanostructured particles and occupational health. J Nanopart Res 7:587–614

Maynard AD, Pui DYH (2007) Nanotechnology and occupational health: new technologies—new challenges. J Nanopart Res 9:1–3

Maynard AD, Aitken RJ, Butz T, Colvin V, Donaldson K, Oberdörster G, Philbert MA, Ryan J, Seaton A, Stone V, Tinkle SS, Tran L, Walker HJ, Warheit D (2006) Safe handling of nanotechnology. Nature 444:267–269

Motzkus C, Macé T, Vaslin-Reimann S (2010) Techniques for characterizing morphology and size of airborne nanoparticles. Congrès Metrology of Airborne Nanoparticles, Standardisation and Applications (MANSA), Abstract Proceeding, 8–9 June 2010, NPL Teddington

Motzkus C, Macé T, Vaslin-Reimann S, Soukiassian L, Ducourtieux D, Michielsen N, Gensdarmes F, Sillon P, Ausset P, Maillé M (2011) Travaux prénormatifs sur la caractérisation des nanoparticules dans l'air : Qualification d'un protocole de génération d'un aérosol nanométrique de SiO_2, Abstract Proceeding, CFA, January 2011, Paris,

Motzkus C, Macé T, Vaslin-Reimann S, Soukiassian L, Ducourtieux D, Michielsen N, Gensdarmes F, Sillon P, Ausset P, Maillé M (2012) Qualification of generation protocol of nanometer aerosol of SiO_2. Revue française de métrologie 29:31–37

Nel A, Xia T, Madler L, Li N (2006) Toxic potential of materials at the nanolevel. Science 311:622–627

Oberdörster G (2001) Pulmonary effects of inhaled ultrafine particles. Int Arch Occup Environ Health 74:1–8

Oberdörster G, Maynard AD, Donaldson K, Castranova V, Fritzpatrick J, Ausman K, Carter J, Karn B, Kreyling W, Lai D, Olin S, Monteiro-Riviere N, Warheit D, Yang H (2005) Principles for characterizing the potential human health effects from exposure to nanomaterials: elements of a screening strategy. Particle Fiber Technol 2:1–35

Rasband WS (1997–2009) Image J, US National Institute of Health, Bethesda, Maryland, USA. http://rsb.info.nih.gov/ij/. Accessed 07 Jan 2013

Rodrigue J, Dhaniyala S, Ranjan M, Hopke PK (2007) Performance comparison of scanning electrical mobility spectrometers. Aerosol Sci Technol 41:360–368

Schmid H, Laskus L, Abraham HJ, Baltensperger U, Lavanchy V, Bizjak M, Burba P, Cachier H, Crow D, Chow J, Gnauk T, Even A, Brink HM, Giesen KP, Hitzenberger R, Hueglin C, Maenhaut W, Pio C, Carvalho A, Putaud J-P, Toom-Sauntry D, Puxbaum H (2011) Results of the carbon conference international aerosol carbon round robin test stage I. Atmos Environ 35:2111–2121

Sebastien P, Billon MA, Janson X, Bonnaud G, Bignon J (1978) Utilisation du microscope électronique à transmission (MET) pour la mesure des contaminations par l'amiante. Arch Mal Prof Med Trav 39:229–248

Slowik JG, Cross ES, Han J-H, Davidovits P, Onasch TB, Jayne JT, Williams LR, Canagaratna MR, Worsnop DR, Chakrabarty RK, Moosmüller H, Arnott WP, Schwarz JP, Gao R-U, Fahey DW, Kok GL, Petzold A (2007) An intercomparison of instruments measuring black carbon content of soot particles. Aerosol Sci Technol 41:295–314

Spurny KR (1994) Sampling analysis, identification and monitoring of fibrous dust and aerosols. Analyst 119:41–51

Tsuji JS, Maynard AD, Howard PC, James JT, Lam CW, Warheit DB, Santamaria AB (2006) Research strategies for safety evaluation of nanomaterials. Part IV: risk assessment of nanoparticles. Toxicol Sci 89:42–50

Wiedensohler A (1988) An approximation of the bipolar charge distribution for particles in the submicron size range. J Aerosol Sci 19:387–389

Wiedensohler A, Aalto P, Covert D, Heintzenberg J, McMurry P (1993) Intercomparison of three methods to determine size distributions of ultrafine aerosols with low number concentrations. J Aerosol Sci 24:551–554

Wiedensohler A, Birmili W, Nowak A, Sonntag A, Weinhold K, Merkel M, Wehner B, Tuch T, Pfeifer S, Fiebig M, Fjäraa AM, Asmi E, Sellegri K, Depuy R, Venzac H, Villani P, Laj P, Aalto P, Ogren JA, Swietlicki E, Roldin P, Williams P, Quincey P, Hüglin C, Fierz-Schmidhauser R, Gysel M, Weingartner E, Riccobono F, Santos S, Grüning C, Faloon K, Beddows D, Harrison RM, Monahan C, Jennings SG, O'Dowd CD, Marinoni A, Horn H-G, Keck L, Jiang J, Scheckman J, McMurry PH, Deng Z, Zhao CS, Moerman M, Henzing B, de Leeuw G (2012) Mobility particle size spectrometers: harmonization of technical standards and data structure to facilitate high quality long-term observations of atmospheric particle number size distributions. Atmos Meas Technol 5:657–685

Witschger O, Fabriès JF (2005) Particules ultra-fines et santé au travail. 1—Caractérisation des effets potentiels sur la santé. INRS, Hygiène et Sécurité au Travail (ND 2227) 199: 21–35

Witschger O, Le-Bihan O, Reynier M, Durand C, Marchetto A, Zimmermann E, Charpentier D (2012) Préconisations en matière de caractérisation des potentiels d'émission et d'exposition professionnelle aux aérosols lors d'opérations mettant en oeuvre des nanomatériaux. INRS, Hygiène et sécurité au travail (ND 2355) 226:41–55

Zervas E, Dorlhène P, Forti L, Perrin C, Momique JC, Monier R, Ing H, Lopez B (2005) Interlaboratory test of exhaust PM using ELPI. Aerosol Sci Technol 39:333–346